Quantifying energy use efficiency via entropy production: A case study from longleaf pine ecosystems

Susanne Wiesner[1], Christina L. Staudhammer[1], Paul C. Stoy[2], Lindsay R. Boring[3,4], Gregory Starr[1]
[1]Department of Biological Sciences, University of Alabama, Tuscaloosa, AL. 35487. USA.
[2]Department of Land Resources and Environmental Sciences, Montana State University, Bozeman, MT 59717, USA
[3]Jones Ecological Research Center, Newton, GA 39870, USA.
[4]Odum School of Ecology, University of Georgia, Athens, GA, 30602, USA

Correspondence to: Gregory Starr (gstarr@ua.edu)

Abstract. Ecosystems are open systems that exchange matter and energy with their environment. They differ in their efficiency in doing so as a result of their location on Earth, structure, and disturbance, including anthropogenic legacy. Entropy has been proposed to be an effective metric to describe these differences as it relates energy use efficiencies of ecosystems to their thermodynamic environment (i.e. temperature), but has rarely been studied to understand how ecosystems with different disturbance legacies respond when confronted with environmental variability. We studied three sites in a longleaf pine ecosystem with varying levels of anthropogenic legacy and plant functional diversity, all of which were exposed to extreme drought. We quantified radiative (eff_{rad}), metabolic and overall entropy changes – as well as changes in exported to imported entropy (eff_{flux}) in response to drought disturbance and environmental variability using 24 total years of eddy covariance data (8 years per site). We show that structural and functional characteristics contribute to differences in energy use efficiencies at the three study sites. Our results demonstrate that ecosystem function during drought is modulated by decreased absorbed solar energy and variation in the partitioning of energy and entropy exports owing to differences in site enhanced vegetation index and/or soil water content. Low eff_{rad} and metabolic entropy, and slow adjustment of eff_{flux} at the anthropogenically altered site prolonged its recovery from drought by approximately one year. In contrast, stands with greater plant functional diversity (i.e., the ones that included both C3 and C4 species) adjusted their entropy exports when faced with drought, which accelerated their recovery. Our study provides a path forward for using entropy to determine ecosystem function across different global ecosystems.

1 Introduction

Ecosystems utilize resources, such as solar radiation, nutrients and water, to maintain a state far from thermodynamic equilibrium (Amthor, 2010; Beer et al., 2009; Finzi et al., 2007; Thomas et al., 2016). Understanding ecosystem resource use efficiency is crucial, as anthropogenic and climate induced changes around the globe continue to alter ecosystem structure and function (Haddeland et al., 2014; Porter et al., 2012; Reinmann and Hutyra, 2016; Thom et al., 2017).

Ecosystems are open and dynamic systems that exchange matter and energy with their surroundings as described by the ecosystem energy balance:

$$R_n = R_{s,in} - R_{s,out} + R_{l,in} - R_{l,out} = LE + H + G + M \quad (1.1)$$

where R_n is net radiation, $R_{s,in}$ and $R_{s,out}$ are incident and upwelling shortwave radiation, and $R_{l,in}$ and $R_{l,out}$ are incoming and upwelling longwave radiation, respectively. The terms LE, H and G represent energy exports through latent heat, sensible heat and ground heat fluxes, respectively and M is an energy storage term comprised of changes in biomass accumulation through metabolic processes (Holdaway et al., 2010). M is often neglected due to the assumption of a steady state over longer periods and because M is much smaller in magnitude compared to other fluxes. However, M imposes a control on energy fluxes, like R_n, LE and H, through changes in leaf area and reflective properties, as well as through active biotic control in response to changes in environmental variables (i.e., stomata opening and closing due to water availability (Hammerle et al., 2013).

From equation 1, ecosystem energy exchange is a function of its thermodynamic environment - the heat transfer of a system with its surroundings - which differs based on the different mechanisms by which heat is transported: conduction, convection, radiation. Complicating our understanding of ecosystem energy dynamics is the fact that more frequent fluctuations in environmental variables are expected as a result of global climate change, including extreme events like droughts, which will alter the resource efficiency of ecosystems across the globe and with it their resilience (Franklin et al., 2016; Woodward et al., 2010).

It is hypothesized that ecosystems aim to optimize their energy use and thus maximize their balance of entropy production and entropy exports to avoid thermodynamic equilibrium (Schneider and Kay, 1994; Schymanski et al., 2010). The magnitude of entropy production and entropy fluxes in ecosystems depend on thermodynamic gradients (i.e., thermal gradients, chemical gradients, etc.) between organisms and their surroundings (Kleidon, 2010). Ecosystems invest energy to build more complex structures (i.e., self-sustainability; Müller and Kroll, 2011; Virgo and Harvey, 2007), which can enhance their entropy export and therefore keep the ecosystem far from thermodynamic equilibrium (Odum, 1988; Schneider and Kay, 1994; Holdaway et al., 2010; Skene, 2015). For example, forest stands with more vertical structure were found to be more efficient in harvesting available light, which consequently increased their productivity (Bohn and Huth, 2017; Hardiman et al., 2011). Productive sites with greater leaf area can maintain higher LE fluxes, which increases their entropy export (Meysman and Bruers, 2010, Brunsell et al., 2011); LE fluxes also maintain lower ecosystem surface temperatures and thereby greater entropy production. On the contrary, large values of H caused by surface temperatures that are greater than air temperatures, result in lower entropy production (LeMone et al., 2007). This has been shown in deforested landscapes (Bonan, 2008; Khanna et al. 2017), as well as comparative studies of different vegetation types and in ecosystems with heterogeneity in their vegetation distribution (Holdaway et al., 2010; Brunsell et al., 2011; Kuricheva et al., 2017).

Here, we evaluate how efficiently ecosystems use energy by assessing ecosystem entropy production as well as by quantifying the ratios in entropy imports and exports (eff_{flux} and dS/dt) in three study ecosystems that represent an edaphic and management gradient. We do so by measuring their structural complexity over an eight-year period via the enhanced vegetation index (EVI) and variation in annual understory biomass, and in relation to the energy and entropy partitioning of incoming energy from solar radiation. We build upon the techniques proposed by Holdaway et al. (2010), Brunsell et al. (2011), and Stoy et al. (2014), by calculating entropy production and entropy fluxes within longleaf pine (*Pinus palustris* Mill.) ecosystems. The sites differed in ecosystem structure (i.e., basal area, Table 1) and plant functional diversity due in part to differences in soil water holding capacity, as well as different levels of anthropogenic legacy. The sites experienced severe drought in the beginning of this

study, which we used to quantify entropy exchanges in response to the disturbance. First, we compare and contrast differences in ecosystem energy fluxes (i.e., R_n, LE, H, G and the net ecosystem exchange of carbon dioxide [NEE]) and entropy fluxes (J_{LE}, J_H, J_G, metabolic entropy [S_m] and radiative entropy production [σ]) in response to changes in structural and environmental variables (EVI, soil water content [SWC], vapor pressure deficit [VPD], and precipitation). Next, we quantify how entropy exports and entropy production at the different sites adjust to changes in incoming entropy when exposed to drought. We do so by estimating radiative efficiency (eff_{rad}), the ratio of entropy production to an empirical maximum entropy production (MEP), and ratios of daily imported and exported entropy fluxes (eff_{flux}), as well as through the overall change in entropy (dS/dt) at the sites. We hypothesize that: (1) the xeric site will have a higher entropy flux from J_H and J_G, but lower S_m due to its lower EVI and lower basal area, which will result in more variable dS/dt compared to the other sites; (2) the mesic site will maintain higher eff_{rad} due to its greater structural complexity (i.e., plant functional diversity and basal area) and thus greater absorptive capacity for solar radiation compared to the other sites; (3) the intermediate site will have lower eff_{rad} and eff_{flux} compared to the mesic and xeric sites, as a result of its lower plant functional diversity (i.e. low abundance of C4 species) and structural complexity, causing lower absorption of solar radiation and export of entropy through LE.

2 Materials and Methods

2.1 Site description

This study was conducted at the Joseph W. Jones Ecological Research Center in southwestern Georgia, USA (31.2201° N, 84.4792° W) from January 2009 to December 2016. The three sites are maintained by frequent low intensity fire on a two-year return interval and were last burned in 2015 (Starr et al., 2016). The climate is humid subtropical with a mean annual precipitation of 1310 mm (Kirkman et al., 2001). Mean temperature extremes range from 3 °C to 16 °C in winter and 22 °C to 33 °C in summer (NCDC, 2011).

The three sites differ based on soil moisture availability as a result of differences in soil drainage. The mesic site lies on somewhat poorly drained sandy loam over sandy clay loam and clay textured soils (Goebel et al., 1997; 2001). Soils at the intermediate site are well drained and have a depth to the argillic horizon of ~165 cm (Goebel et al., 1997). The xeric site lies on well-drained deep sandy soils with no argillic horizon (Goebel et al., 1997). All sites are situated within 10 km of each other and have average elevations of 165, 155, and 160 m for the mesic, intermediate, and xeric sites, respectively.

Ninety-five-year-old longleaf pine trees (*Pinus palustris* Mill.) dominate the overstory of all sites, and overall basal area (B_A) and diameter at breast height (DBH) varied by site (Table 1). The overstories of each site also contain a small proportion of oak trees; the xeric site has the highest proportion with 22 %, versus 8 % and 7.7 % at the mesic and intermediate sites, respectively. The understory at the mesic and xeric sites is largely covered with perennial C_4 grass species, such as wiregrass (*Aristida beyrichiana* [Trin.]), whereas woody species dominate the intermediate site. Composition and abundance of other plant species varies by site (Kirkman et al., 2001; 2016). Soil perturbation at the intermediate site affected species richness, so that wiregrass is almost absent.

We acquired EVI for 2009 through 2016 for all three sites from the online data pool at lpdaac.usgs.gov via the NASA Land Processes Distributed Active Archive Center (LP DAAC) and the USGS Earth Resources Observation and Science Center

(EROS), using MODIS Aqua and Terra data products (MYD13Q1 and MOD13Q1; DAAC, 2008) to quantify changes in ecosystem structure from disturbance. EVI products for the sites were available on an eight-day basis and linearly interpolated to obtain daily estimates. We also acquired Palmer Drought Severity Indices (PDSI) for Southwest Georgia from the National Oceanic and Atmospheric Administration data archive for 2009 to 2016 to identify the months of drought disturbance (Dai et al., 2004).

Understory composition and biomass was estimated annually from 2009 through 2013. Thereafter, the collection frequency became biannual, so that 2014 and 2016 were missing in the data collection. Understory biomass was estimated using 0.75 m^2 clip plots, which were randomly located by tossing a plot frame from pre-installed litter trap positions (n = 20 per site; see Wiesner et al. 2018). All live and dead vegetation, smaller than 1 m in height was clipped and analyzed in our laboratory. Vegetation was classified by plant life form (here, forbs, ferns, legumes, wiregrass, other grasses, and woody plants), and each sample was dried to constant weight.

Net ecosystem exchange of CO_2 measurements. Net ecosystem exchange (NEE) was measured continuously at 10 Hz at all three sites from January 2009 to December 2016 using open-path eddy covariance (EC) techniques (Whelan et al., 2013). Data were stored on CR-5000 dataloggers (Campbell Scientific, Logan, UT). CO_2 and water vapor concentration were measured with an open path infrared gas analyzer (IRGA, LI-7500, LI-COR Inc., Lincoln, NE) and wind velocity and sonic temperature were measured with a three-dimensional sonic anemometer (CSAT3, Campbell Scientific, Logan, UT). These sensors were installed ~4 m above mean canopy height at each site (34.5, 37.5, and 34.9 m for the mesic, intermediate and xeric sites, respectively), ~0.2 m apart to minimize flow distortion between the two instruments and vertically aligned to match the sampling volume of both instruments.

2.2 Sensible and latent heat flux measurements

Net energy fluxes of LE and H were estimated in W m^{-2} using temperature and wind velocity measurements from the sonic anemometer, as well as water vapor density measurements from the IRGA:

$$LE = \lambda \rho_a \overline{w'q'} \quad (2.1)$$

$$H = \rho_a c_p \left(\overline{w'T_s'} - 0.000321 T_s \overline{w'q'}\right) \quad (2.2)$$

where λ is the latent heat of vaporization (J kg^{-1}), ρ_a is the density of air (kg m^{-3}), c_p is the specific heat of air (kJ kg_{-1} K^{-1}), w' is the instantaneous deviation of vertical wind speed (w, m s^{-1}) from the mean, and q' and T_s' are the instantaneous deviations of water vapor concentration (kg kg^{-1}) and sonic temperature (Kaimal and Gaynor, 1991) from their respective means. The overbars in Eqs. 2.1 and 2.2 signify the time-averaged covariance. Missing H and LE were gap-filled on a monthly basis using simple linear models as a function of R_n.

In cases where energy balance closure was not achieved, energy fluxes of H and LE were corrected using the Bowen method following Twine et al. (2000), where fluxes are adjusted using residual energy, and the estimated Bowen ratio ($\beta = H/LE$), which assumes that β was correctly measured by the EC system:

$$LE = \frac{1}{1+\beta}(R_n - G) \quad (2.3)$$

$$H = \beta \times LE \quad (2.4)$$

Closing the energy balance is important to quantify differences in energy and entropy fluxes by site, as according to the First law of Thermodynamics energy is always conserved. To quantify differences in environmental drivers and site variation between energy and entropy fluxes, we established models of average daily energy fluxes (described in section 2.7)

2.3 Meteorological instrumentation

Meteorological data above the canopy were also collected and stored on the CR-5000 dataloggers (Campbell Scientific, Logan, UT). Meteorological data measured on the towers included: photosynthetically active radiation (PAR; LI-190, LI-COR Inc., Lincoln, NE), global radiation (LI-200SZ, LI-COR Inc., Lincoln, NE), incident and outgoing shortwave and longwave radiation to calculate R_n (NR01, Hukseflux, thermal sensors, Delft, The Netherlands), precipitation (TE525 Tipping Bucket Rain Gauge, Texas Electronics, Dallas, TX), wind direction and velocity (Model 05103-5, R.M. Young, Traverse City, MI), air temperature (T_{air}) and relative humidity (RH; HMP45C, Campbell Scientific, Logan, UT), and barometric pressure (PTB110, Vaisala, Helsinki, Finland).

Soil temperature (T_{soil}), volumetric water content of the soil (SWC) and soil heat flux (G) were measured in one location near the base of each tower at each site every 15 seconds and averaged every 30 minutes on an independently powered CR10X datalogger. T_{soil} was measured at depths of 4 and 8 cm with insulated thermocouples (Type-T, Omega Engineering, INC., Stamford, CT), and G was measured at a depth of 10 cm with soil heat flux plates (HFP01, Hukesflux, Delft, The Netherlands). SWC was measured within the top 20 cm of the soil surface using a water content reflectometer probe (CS616, Campbell Scientific, Logan, UT).

2.4 Data processing

Raw EC data were processed using EdiRe (v.1.4.3.1184; Clement, 1999), which carried out a two-dimensional coordinate rotation of the horizontal wind velocities to obtain turbulence statistics perpendicular to the local streamline. Fluxes were calculated for half-hour intervals and then corrected for mass transfer resulting from changes in density not accounted for by the IRGA. Barometric pressure data were used to correct fluxes to standard atmospheric pressure. Flux data screening was applied to eliminate 30-min fluxes of NEE, H and LE, resulting from systematic errors as described in Whelan et al. (2013) and Starr et al. (2016). Such errors encompassed (amongst other things): rain, poor coupling of the canopy and the atmosphere (defined by the friction velocity, ustar), and excessive variation from half-hourly means.

Gross ecosystem exchange (GEE) and ecosystem respiration (R_{eco}) were estimated from eddy covariance measurements of net ecosystem exchange of CO_2 (NEE; μmol m^{-2} s^{-1}) at a time resolution of half an hour, from which GEE and R_{eco} can be estimated as follows:

$$GEE = -NEE + R_{eco} \quad (2.5)$$

Missing half hourly data were gap-filled as described in Whelan et al. (2013) and Starr et al. (2016). Daytime and nighttime data were estimated utilizing a Michaelis-Menten approach for (PAR > 10 μmol m^{-2} s^{-1}) and a modification of the Lloyd and Taylor (1994) model (PAR ≤ 10 μmol m^{-2} s^{-1}), respectively. Monthly equations were used to gap-fill data; however, where too

few observations were available to produce stable and biologically reasonable parameter estimates, annual equations were used. NEE partitioning to estimate daytime R_{eco} was performed by using the nighttime gap-filling equation, and then utilizing equation (2.5) to estimate GEE. Nighttime GEE was assumed to be zero.

2.5 Entropy production calculations

Half-hourly GEE and R_{eco} were converted to W m^{-2} (GEE_e and R_{eco_e}), using the assumption that one micromole of CO_2 stores approximately 0.506 J, where 1 J m^{-2} s^{-1} equals 1 W m^{-2} (Nikolov et al., 1995), which is then released during respiration.

For entropy production and fluxes of shortwave (R_s) and longwave radiation (R_l) we followed established approaches of Brunsell et al. (2011), Holdaway et al. (2010), and Stoy et al. (2014). The half-hourly entropy flux produced through absorption of R_s emitted by the surface of the sun (J_{Rs}, W m^{-2} K^{-1}) was calculated as:

$$J_{Rs} = \frac{R_{s,net}}{T_{sun}} \quad (2.6)$$

where sun surface temperature (T_{sun}) was assumed to be 5780 K, with $R_{s,net}$ defined as the difference of incident and upwelling R_s. The entropy flux of R_l (J_{Rl}, W m^{-2} K^{-1}) was calculated as:

$$J_{Rl} = \left(\frac{R_{l,in}}{T_{sky}} - \frac{R_{l,out}}{T_{srf}}\right) \quad (2.7)$$

where $R_{l,in}/T_{sky}$ is the entropy flux of $R_{l,in}$ as incoming R_l ($J_{Rl,in}$), and $R_{l,out}/T_{srf}$ is the entropy flux of $R_{l,out}$ as outgoing R_l ($J_{Rl,out}$).

Surface temperature (T_{srf}; K) was calculated from upwelling R_l ($R_{l,out}$):

$$T_{srf} = \left(R_{l,out} \Big/ (A \times e_{srf} \times k_B)\right)^{1/4} \quad (2.8)$$

with emissivity of the surface calculated as e_{srf} = 0.99-0.16α (Juang et al., 2007), the view factor A was assumed to be unity, and the Stefan-Boltzmann constant $k_B = 5.67 \times 10^{-8}$ W m^{-2} K^{-4}. The shortwave albedo (α) was calculated as the daily average of noontime outgoing R_s ($R_{s,out}$) divided by $R_{s,in}$. The sky temperature, T_{sky} (K), was calculated from $R_{L,in}$ using the Stefan-Boltzmann equation:

$$T_{sky} = \left(R_{l,in} \Big/ (A \times e_{atm} \times k_B)\right)^{1/4} \quad (2.9)$$

where the emissivity of the atmosphere (e_{atm}) was assumed to be 0.85, following Campbell and Norman (1998).

All other ecosystem entropy fluxes J_{LE}, J_H, J_G, and J_{GEE} and J_{Reco} (W m^{-2} K^{-1}) were calculated by dividing the energy fluxes by temperature as:

$$J_x = \frac{x}{T_y} \quad (2.10)$$

where x = LE, H, G and GEE_e and R_{eco_e}, and T_y = was assumed to be T_{air} (for J_{LE}, J_H, J_{GEE} and J_{Reco}; K) or T_{soil} (for J_G, in K).

We also calculated entropy produced from evaporation associated with mixing of saturated air from the canopy with the fraction of air in the atmosphere that has RH below 100 % (JLE_{mix}), following Holdaway et al. (2010):

$$JLE_{mix} = ET \times R_v \times \ln(RH) \quad (2.11)$$

where the evapotranspiration rate is calculated as $ET = LE/\lambda$ (kg m^{-2} s^{-1}) and R_v is the gas constant of water vapor (0.461 kJ kg^{-1} K^{-1} for moist air).

The sum of entropy of ecosystem fluxes (J, W m^{-2} K^{-1}) for each half-hour was then calculated by adding all entropy fluxes between the surface and atmosphere:

$$J = J_{Rl} + J_{Rs} + J_{LE} + J_H + J_G + J_{GEE} + J_{Reco} + JLE_{mix} \quad (2.12)$$

The conversion of low entropy R_s and R_l to high entropy heat at the surface through absorption of R_s and R_l, respectively, was calculated as:

$$\sigma_{Rs} = R_{s,net}\left(\frac{1}{T_{srf}} - \frac{1}{T_{sun}}\right) \quad (2.13)$$

$$\sigma_{Rl} = R_{l,in}\left(\frac{1}{T_{srf}} - \frac{1}{T_{sky}}\right) \quad (2.14)$$

where T_{srf} is the radiometric surface temperature (Eq. 2.8) and σ_{RS} and σ_{Rl} are in W m^{-2} K^{-1}.

The overall half-hourly entropy production (σ, W m^{-2} K^{-1}) was then calculated as the sum of the entropy productions of R_s and R_l:

$$\sigma = \sigma_{Rl} + \sigma_{Rs} \quad (2.15)$$

We excluded the factor 4/3, which is associated with the transfer of momentum exerted by electromagnetic radiation on a surface (Wu et al., 2008), in our calculations of σ and J for entropy production and entropy fluxes because we assumed that radiation pressure at the sites would be negligible (see Ozawa et al. 2003; Kleidon and Lorenz, 2005; Fraedrich and Lunkeit, 2008; Kleidon, 2009; Pascale et al., 2012).

To account for the difference in absorbed radiation on leaf and non-vegetated surfaces, we partitioned σ using EVI as an approximation for fractional vegetation cover. Accordingly, σ of non-vegetated surfaces (σ_{land}) was estimated as:

$$\sigma_{land} = (1 - EVI) \times \sigma \quad (2.16)$$

Entropy production on leaf surfaces (σ_{leaf}, eq. 2.17) was calculated as the sum of entropy production (σ_{PAR} eq. 2.18) from absorbed photosynthetic active radiation (FPAR in W m^{-2}, eq. 2.19), and entropy production from the remainder of R_s-PAR ($\sigma_{Rs,leaf}$, eq. 2.20), assuming all was absorbed and converted into heat on leaf surfaces, as well as entropy production from absorbed longwave radiation on leaf surfaces (eq. 2.21).

$$\sigma_{leaf} = \sigma_{PAR} + \sigma_{Rs,leaf} + \sigma_{Rl,leaf} \quad (2.17)$$

where,

$$\sigma_{PAR} = FPAR\left(\frac{1}{T_{air}} - \frac{1}{T_{sun}}\right) \quad (2.18)$$

$$FPAR = EVI \times PAR \quad (2.19)$$

$$\sigma_{Rs,leaf} = (R_s - PAR)\left(\frac{1}{T_{air}} - \frac{1}{T_{sun}}\right) \times EVI \quad (2.20)$$

$$\sigma_{Rl,leaf} = \sigma_{Rl} \times EVI \quad (2.21).$$

We assumed T_{air} was close to leaf temperature. While this formulation may introduce assumptions about the absorptive behavior of leaves, it helps us to estimate entropy production from the metabolic processes of photosynthesis and respiration (S_m) as follows:

$$S_m = \sigma_{leaf} + J_{GEE} + J_{Reco} \quad (2.22)$$

Finally, we estimated half-hourly change in entropy production (S) over time (t) in W m^{-2} K^{-1} of the ecosystem by adding entropy flux of imports ($J_{Rs,net}$, $R_{Rl,in}$) and exports (i.e., J_{LE}, J_H, J_G, J_{GEE}, J_{Reco}, $J_{Rl,up}$, JLE_{mix}) and entropy production of vegetated and non-vegetated surfaces:

$$dS/dt = J + \sigma_{land} + \sigma_{leaf} \quad (2.23)$$

Note that this approach does not account for entropy production due to frictional dissipation of entropy from rainfall or subsurface water flow, as these would be of even smaller magnitude than entropy production from metabolic activity of the ecosystem (Brunsell et al., 2011). Here negative dS/dt represents the export of entropy of the ecosystem to its surroundings.

2.6 Ecosystem entropy models for radiation and ecosystem fluxes

We estimated half-hourly MEP of the radiation budget (MEP_{rad}) in W m^{-2} K^{-1}, to compare site differences in radiation energy use and entropy dissipation.

Empirical MEP (MEP_{rad}) was determined following Stoy et al. (2014), by estimating the MEP of half-hourly R_s (MEP_{Rs}) and R_l (MEP_{Rl}):

$$MEP_{Rs} = R_{s,in}\left(\frac{1}{T_{srf}} - \frac{1}{T_{sun}}\right) \quad (2.23)$$

$$MEP_{Rl} = R_{l,net}\left(\frac{1}{T_{srf}} - \frac{1}{T_{air}}\right) \quad (2.24)$$

$$MEP_{rad} = MEP_{Rs} + MEP_{Rl} \quad (2.25)$$

This method offers a means to compare different sites with respect to their reflective and absorptive capacities *versus* a reference ecosystem that absorbs and dissipates all incident solar energy. Note that MEP_{Rl} is often of lower magnitude than MEP_{Rs} because here we assume that an efficient ecosystem would dissipate less energy through sensible heat, such that T_{srf} would approach T_{air}.

The half-hourly entropy ratio of radiation is then calculated using σ_{land} and σ_{leaf} as follows:

$$eff_{rad} = \frac{\sigma_{land}+\sigma_{leaf}}{MEP_{rad}} \quad (2.26).$$

We refer to this ratio as an efficiency to describe differences in the absorptive characteristics at the sites, where a ratio closer to 1 would indicate high radiation absorption. Furthermore, sites that maintain lower surface temperatures through greater LE fluxes would also increase their entropy production, thus linking ecosystem functional efficiency with radiative entropy production. We then estimated the variable eff_{flux} as the ratio of incoming radiation entropy (J_{Rs} and $J_{Rl,in}$) and the sum of exported entropy fluxes (J_{LE}, J_H, J_G, J_{GEE}, J_{Reco}, and $J_{Rl,up}$) to assess how entropy was partitioned into entropy production and entropy fluxes over the different study years.

2.7 Statistical analyses

We estimated average daily values for all response variables to decrease autocorrelation for statistical analysis. We first tested for significant differences in environmental and structural variables among the three sites prior to the entropy analysis. We estimated simple general linear mixed models (GLMM) using the R package *nmle* to look at differences among sites for: rain, SWC, vapor pressure deficit (VPD), EVI, T_{srf}, T_{air}, T_{sky} and T_{soil}, as well as $R_{s,in}$, $R_{s,out}$, $R_{l,in}$ and $R_{l,out}$. All response variables were daily means. For rainfall we calculated monthly sums to estimate differences among the sites. We included a random effect for day of measurement, to account for repeated measurements, as well as an AR(1) structure to account for temporal autocorrelation among measurements. The model of rainfall only included year and site as independent variables and no random effects. Independent variables for the other models were month, year and site, as well as their interactions.

Subsequently, we estimated GLMMs of daily energy (R_n, LE, H, G and NEE_e) and entropy fluxes (J_{LE}, J_H, J_G, and S_m), entropy production (σ), entropy ratios (eff_{rad} and eff_{flux}) and overall entropy (dS/dt) to quantify their differences by environmental and structural variables by site. For all models we included random effects and an AR(1) autoregressive correlation structure to account for repeated daily measurements. All models initially included independent variables for site, year and month, mean EVI, SWC, VPD and daily rainfall sums. We also included interactions of environmental variables with site, site with year and site with month, to determine changes in the energy efficiency over the study period among sites. Independent variables and their interactions were deemed significant when $p<0.05$. We used a Tukey adjustment to test for significant differences among sites. GLMM analyses were performed via the R packages *nlme*, *lsmeans*, and *car* (Fox and Weisberg, 2011; Lenth, 2016; Pinheiro et al., 2014).

3 Results

3.1 Differences in environmental, radiative and temperature variables among sites

All three sites experienced a severe drought from mid-2010 through mid-2012 (Fig. S1, Supplementary Information). There was no significant difference between the mesic and xeric sites in rainfall sums, but the intermediate site had lower rainfall sums (~20 mm per month) compared to the other sites (Table S1). SWC was significantly lower at the xeric (<19 %) compared to mesic and intermediate sites (~20 %) for all years of this study (Fig. 1a and b, Table S2). SWC and EVI decreased during the drought at all sites, but only significantly so at the mesic site. VPD significantly increased at all sites during the drought. For all years, EVI was significantly lower (0.02-0.04) at the xeric site compared to the other two sites (Fig. 1e and f), while the intermediate site had significantly higher EVI compared to the mesic site, except in 2010.

Daily T_{srf} at the mesic site was significantly higher than the xeric site for all years except 2012, 2014 and 2016 (Fig. 2a). From 2012 to 2016 the intermediate site had higher T_{srf} compared to the other two sites. T_{air} was significantly lower at the mesic site compared to the intermediate and xeric sites for all years, except in 2012, and in 2014, when the xeric site had higher T_{air} compared to the intermediate (Fig. 2a). T_{soil} was significantly lower at the mesic site compared to the other sites, except in 2013, when there was no significant difference between the mesic and xeric sites. For all years, daily T_{soil} was significantly

higher at the xeric site compared to the intermediate site except for 2011 and 2012, when the intermediate site was significantly higher.

$R_{s,out}$ was significantly higher at the xeric site compared to the other sites, except for 2014, where we found no significant difference between the intermediate and xeric sites. Daily $R_{s,out}$ was also significantly lower at the mesic site, compared to the intermediate site, except in 2009. Average daily $R_{l,out}$ was significantly lower at the mesic site compared to the intermediate site during all years, except for 2011 and 2012, and compared to the xeric site for all years, except for 2011. The intermediate site had significantly higher $R_{l,out}$ compared to the xeric site during 2013, 2014 and 2016. As a consequence of these component fluxes, R_n was significantly higher at the xeric site compared to the intermediate site for all years except 2009 and 2014 (SI Fig. S2a, Table S3). Average R_n was significantly lower at the mesic site compared to the xeric site in 2013 and 2016, and was significantly higher compared to the xeric site from 2009 to 2011. Average daily R_n significantly increased at the intermediate and xeric sites but showed no change at the mesic site with an increase in EVI (SI Fig. S3a).

Environmental, radiative and temperature variables also tended to be significantly different among months within site, and in many instances among sites by month. Differences followed seasonal patterns, as noted in SI Fig. S2 and SI Table S2.

3.2 Understory wiregrass and woody abundance at the sites

Wiregrass was virtually absent at the intermediate site for all years of this study (Fig. 4a), whereas woody species were more abundant compared to the others. The mesic and xeric sites both had higher proportions of wiregrass in the understory (~25 % versus 5 % at the intermediate site), which slightly decreased during 2011 (Fig. 4a). In addition, woody biomass increased to ~75 g m^{-2} at the xeric site during 2011, but not at the mesic site. In 2012, woody biomass decreased to ~40 g m^{-2} at the xeric and intermediate sites and remained low during the following years at the xeric site, but increased at the intermediate site (>100 g m^{-2}, Fig. 4b).

3.3 Energy fluxes of H, LE, and G

LE was significantly lower at the intermediate site compared to the mesic site for all years, except 2011, and compared to the xeric site for all years, except for 2015. We found no significant difference between the mesic and xeric sites in 2009, 2010, 2014 and 2016, but for the other years of this study the xeric site had significantly higher LE. LE significantly increased at all sites with higher EVI, with a greater increase at the intermediate and a smaller increase at the xeric site, compared to the mesic site (SI Fig. S3g). LE significantly increased at all sites with an increase in SWC and VPD (SI Fig. S3e and f). LE at the intermediate site was significantly lower compared to the other sites for all levels of VPD (SI Fig. S3g). LE was significantly lower with higher rainfall, with no significant differences among sites (SI Fig. S3h).

There was no significant difference in H between the mesic and intermediate sites, except in 2011 and 2013, when the mesic site was higher than the intermediate, and in 2015 and 2016, when the reverse occurred. H was significantly lower at the xeric site compared to the mesic site for all years except for 2014 and 2016, and compared to the intermediate site for all years except 2011 and 2013. Average H was significantly higher at the mesic site compared to the xeric site during the months of May through October (SI Fig. S2b). The intermediate site had significantly lower H compared to the other two sites for the

months of January through March and the xeric site had significantly lower H for June through October. Compared to the other two sites, average H was significantly lower at the intermediate site when EVI was greater than 0.4, and significantly higher at the xeric site for EVI > 0.5 (SI Fig. S3i). Average H significantly decreased at all sites with an increase in SWC (SI Fig. S3j). Average daily H significantly increased at all sites with an increase in VPD, with a lower decrease at the intermediate site (SI Fig. S3k).

G was significantly lower at the intermediate site during 2016 (negative), compared to 2009 through 2011 and 2014. Average daily G was positive during summer months, and negative during winter months (October through March) at all sites (SI Fig. S2b). Average daily G significantly decreased with an increase in EVI at the mesic and intermediate site, but had no significant change at the xeric site (SI Fig. S3m). G was significantly less positive at the xeric site compared to the other sites for EVI < 0.3, but was significantly more negative at the intermediate site compared to the mesic and xeric sites when EVI was above 0.4. Average G significantly decreased (to negative) with an increase in SWC (SI Fig. S3n), and significantly increased (to positive) with an increase in VPD, but only at the intermediate and xeric sites (SI Fig. S3o). Daily rainfall did not significantly alter G at the sites, but the intermediate site had significantly more negative G compared to the other two sites (2-10 W m^{-2}) when daily rainfall was positive (SI Fig. S3p).

3.4 Entropy production and fluxes of J_H, J_{LE}, and J_G

For all years, average daily σ (as the sum of σ_{land} and σ_{leaf}) was significantly higher at the mesic site compared to the intermediate site (by > 0.01 – 0.036 W m^{-2} K^{-1}; Fig. 5a, Table S4), while σ was not significantly different between the mesic and xeric sites for almost all years (Fig 5a). Average daily σ significantly increased with EVI, independent of site (Fig. 6a), and also significantly increased with SWC and VPD, with a greater slope at the xeric site (Fig. 6b and c). Average daily σ significantly decreased at all sites with an increase in rainfall (noting that entropy production from rainfall itself is not considered here and assumed to be approximately equal among ecosystems), and σ was significantly lower at the intermediate site during rainy periods compared to the other two sites (Fig. 6d). There was no significant difference in σ at the mesic and xeric sites for all levels of rain.

The xeric site had significantly higher average daily J_{LE}, ranging from ~0.22 to 0.28 W m^{-2} K^{-1}, versus the intermediate site with ~0.18 – 0.25 W m^{-2} K^{-1} (Fig. 5a, Table S4) for all years, except 2015. J_{LE} at the xeric site was also higher than the mesic site in 2011 through 2013 and in 2015, ranging from 0.2 to 0.26 W m^{-2} K^{-1}. The mesic site had ~0.01-0.06 W m^{-2} K^{-1} higher J_{LE} compared to the intermediate site, except in 2011. J_{LE} significantly increased with greater EVI and SWC (Fig. 6e and f). J_{LE} was significantly higher at the xeric site compared to the other sites for EVI < 0.4. J_{LE} was significantly higher at the xeric site compared to the other sites when SWC was above 19%, similar to the model of LE. J_{LE} significantly increased with VPD, and significantly decreased with rainfall (Fig. 6g and h). Unlike the model results for LE, the effects of VPD were not significantly different by site.

Models of H and J_H were similar, except that J_H in the mesic and xeric sites were not significantly different in 2015 (Fig. 5a, Table S4). Average daily J_H was significantly higher at the mesic site in 2011 and 2012 (~0.2-0.24 W m^{-2} K^{-1}) compared to the intermediate (~0.19 W m^{-2} K^{-1}; Fig. 5a) and xeric sites (~0.16-0.20 W m^{-2} K^{-1}). In 2009, 2010 and 2012, the xeric site had

significantly lower J_H compared to the other sites (by ~ 0.02 W m^{-2} K^{-1}). J_H decreased only at the mesic and intermediate sites with increasing EVI (Fig. 6i) such that the intermediate site had significantly lower J_H compared to the other sites when EVI was above 0.4. J_H decreased with increased SWC at all sites, and the xeric site had significantly lower J_H compared to the other sites when SWC was above 19 % (Fig. 6j). VPD significantly increased J_H at all three sites, with a greater increase at the xeric site (Fig. 6k). J_H significantly decreased at all sites with increased rainfall, where the intermediate site had significantly lower J_H compared to the mesic and xeric sites when rainfall was greater than 40 mm per day (Fig. 6l).

Average daily J_G was not significantly different among the years 2009-2014 and 2016 at the mesic site, but significantly increased during 2015 (Fig. 5a, Table S4), similar to the model results for G. Similarly, J_G was significantly lower at the intermediate site during 2016 (negative). J_G at the xeric site was not significantly different by year. Average daily J_G was positive during summer months, and negative during winter months at all sites (Fig. 5b). Average daily J_G significantly decreased from positive to negative at the mesic and intermediate sites with an increase in EVI, with no significant change at the xeric site (Fig. 6m), similar to the model of G. J_G was significantly more negative at the intermediate site compared to the other sites for EVI > 0.4. Average J_G only significantly decreased at the intermediate and xeric sites (to negative), such that J_G was significantly more negative at the two sites when SWC was above 18% (Fig. 6n). J_G significantly increased with greater VPD, independent of site (Fig. 6o). Similar to the model of G, daily rainfall did not significantly alter the magnitude of J_G at the sites. However, the intermediate had significantly more negative J_G compared to the other two sites when daily rainfall increased (Fig. 6p).

3.5 Metabolic energy and entropy

Metabolic energy was consistently more negative (more energy uptake) at the mesic site, compared to the other sites for all years in this study (Fig 7a, Table S5). The intermediate and xeric sites exported metabolic energy from 2009 through 2011, which was greater at the intermediate site for 2010. NEE_e significantly increased to more negative at all sites during May and significantly decreased during August through October, which resulted in positive NEE_e at the intermediate site (Fig. 7b). NEE_e significantly decreased at all sites with an increase in EVI, which was greater at the xeric site (Fig. 7c). An increase in SWC resulted in decreasing NEE_e, independent of site (Fig. 7d). An increase in VPD significantly decreased NEE_e to more negative at all sites, with a greater decrease at the intermediate site (Fig. 7e). Increases in rainfall significantly increased NEE_e to positive at all sites, where the intermediate site had a greater increase compared to the other sites (Fig. 7f).

Results of the model of S_m indicated that the mesic site had significantly greater metabolic entropy production compared to the intermediate site for all years but 2009 and 2013. The xeric site had significantly greater S_m compared to the mesic site in 2012 through 2014 and in 2016, and compared to the intermediate site for all years (Fig. 7g). S_m was greater during summer months at all sites with no significant differences between the mesic and xeric sites from February through August, but significantly lower at the intermediate site compared to the xeric site for all months (Fig. 7h, Table S5). Metabolic entropy production was significantly lower at the intermediate site compared to the mesic site for most months except January, April, October and December. Values of S_m significantly increased with an increase in EVI, independent of site (Fig. 7i). SWC significantly increased S_m at all sites, with a greater slope at the xeric site (Fig. 7j). Higher VPD significantly increased S_m

similar to the model of NEE_e; however slopes were more similar among the sites (Fig. 7k). Rainfall significantly decreased S_m to ~0 with a greater slope at the intermediate site, similar to the model of NEE_e (Fig. 7l).

3.6 Entropy models

From 2011 through 2016, eff_{rad} was significantly higher at the mesic site (0.89-0.93), compared to the intermediate (0.88-0.91) and xeric (0.88-0.92) sites, which were not significantly different (Fig. 8a). Average eff_{rad} did not significantly change with EVI or SWC. Higher VPD significantly decreased values of eff_{rad} at all sites (Fig. 8c). The mesic site had significantly higher values of eff_{rad} compared to the other two sites for all levels of VPD (Fig. 8c). Rainfall significantly increased values of eff_{rad} at all sites, with a greater increase at the intermediate site (Fig. 8d, Table S6).

Daily average eff_{flux} was significantly greater at the mesic site for most of the measurement period (Fig. 9a, Table S6). eff_{flux} was significantly higher at the xeric site compared to the intermediate site for the years 2009, 2011, and 2013 through 2015. For 2012 and 2016 the intermediate site had significantly greater eff_{flux} compared to the xeric site. Greater EVI only significantly increased eff_{flux} at the mesic site, which had higher eff_{flux} compared to the other sites for all levels of EVI (Fig. 9c). The intermediate site had significantly lower eff_{flux} compared to the xeric site when EVI was above 0.3. An increase in SWC significantly decreased values of eff_{flux} only at the intermediate and xeric sites, with a greater decrease at the xeric site (Fig. 9d). Higher VPD significantly decreased eff_{flux} at all sites, with a greater decrease at the intermediate site (Fig. 9e). Rainfall significantly increased eff_{flux} at all sites, where the intermediate site showed the highest increase (Fig. 9f).

There was no significant difference in dS/dt among sites for all years and months, except in 2014, where the intermediate site had significantly higher dS/dt compared to the other sites (Fig. 10a, Table S6). In addition, the xeric site accumulated dS/dt during 2012 such that it was significantly different from the other sites. An increase in VPD resulted in a significant increase in dS/dt (more entropy export), independent of site (Fig. 10c). EVI, SWC and rainfall were not significant in the model of dS/dt. The diurnal variation in dS/dt was greater at the mesic and xeric sites during the drought years 2010, 2011 and 2012, compared to the intermediate site, specifically during nighttime (SI Fig. S4). At the intermediate site dS/dt varied more during the years 2014 and 2016, as seen by greater entropy accumulation during nighttime hours and greater export during daytime hours for the year 2014.

4 Discussion

Here we describe differences in energy use efficiencies of sites with varying structural complexities (i.e., understory composition, basal area, DBH) using metrics of energy and entropy. Different from our expectations, environmental and structural effects on energy and entropy fluxes were not different with the exception of NEE_e and S_m. These results suggest that differences in the thermodynamic environment among sites (i.e., air and surface temperatures) did not contribute to changes in entropy export in response to environmental variables. Metabolic entropy (S_m) decreased during the drought at all sites, but not significantly so (Fig. 7), whereas NEE_e showed significant change at the mesic site. The different results were a function of SWC, which decreased during the summer of 2011, thus lowering the flux of S_m (Fig. 7). Furthermore, greater

$R_{s,out}$ during the drought indicated lower available energy to drive photosynthetic processes. The decreases in S_m and NEE_e suggest that metabolic activity was affected by low rainfall, increasing VPD, and changes in temperature, demonstrating lower physiological activity of plant species during drought (Barron-Gafford et al., 2013). This decrease in metabolic efficiency supports a previous study at the mesic and xeric sites, which found lower electron transport and carboxylation capacity during drought (Wright et al., 2012).

Differences in the underlying reflective capacities at the sites significantly altered their entropy production and resulted in variation in entropy exchanges (Stoy et al., 2014). The more structurally complex mesic site had greater metabolic entropy production (S_m) compared with the intermediate site. Greater S_m at the mesic site translates to greater energy accumulation, in addition to greater radiation entropy and export efficiencies (eff_{rad}, eff_{flux}) compared to the intermediate site, which had greater land use legacy and was structurally similar, but lower in plant functional diversity. Although the radiation entropy ratio (eff_{rad}) indicated that both the intermediate and xeric sites were equally energy efficient in terms of absorbing radiation, eff_{flux} and S_m showed prolonged recovery of energy efficiency from drought by one year at the intermediate site. Entropy change over time (dS/dt) did not significantly vary at the mesic site, but was more variable at the xeric and intermediate sites following the drought.

We hypothesized that the xeric site would have higher H and J_H, due to its open canopy and sandy soils and therefore lower volumetric heat capacity. In contrast to our first hypothesis, the mesic and intermediate sites and not the xeric site had a more pronounced increase in H and J_H when EVI decreased during drought (Fig. 1). Lower H and J_H at the xeric site was a consequence of greater energy partitioning into LE, enabled by greater transpiration rates of plant functional types present at the site (deciduous and evergreen oaks in the understory, mid- and overstory; Klein et al., 2013; Renninger et al., 2015; Stoy et al., 2006). This result was confirmed, as J_H fluxes did not significantly change with an increase in EVI, whereas J_{LE} increased, suggesting that evapotranspiration and the cooling of leaf and soil surfaces had greater influence on the partitioning of available energy. In contrast, J_H increased more at the mesic and xeric sites with increasing VPD, suggesting that drier air increased the sensible heat flux from the surface to the atmosphere (Massmann et al., 2018). Similarly, as VPD increased so did σ at all sites. This response was also observed in Kuricheva et al. (2017), where drier summers resulted in greater entropy production, likely because an increase in VPD correlated with greater absorption of solar radiation and partitioning to H (Fig. 3a). Even though plant abundance was lower at the xeric site, its species composition was better adapted to drought conditions, which allowed for higher J_{LE} compared to the other sites (Roman et al., 2015). Furthermore, an increase in EVI during summer months at the xeric site increased J_{LE}, demonstrating that greater leaf area enhanced ecosystem function (Peng et al., 2017; Zhu et al., 2016). Interestingly, J_{LE} did not vary significantly by site with changes in VPD, which supported the findings of Whelan et al. (2013) that all sites had similar stomatal regulation to increases in VPD. Overall, the xeric site had higher J_{LE} compared to the other sites for EVI < 0.5, even though the site basal area was almost half that of the mesic and intermediate sites (Table 1). An overstory composed of more oak species at the xeric site (~20 %) along with the C_4 understory resulted in higher transpiration during spring and summer, compared to stands containing just pine trees (Klein et al., 2013; Renninger et al., 2015; Stoy et al., 2006). Additionally, C_4 grasses and oak species at the xeric site were better adapted to drought (i.e., anisohydric response; Osborne and Sack, 2012; Roman et al., 2015), which may enable higher entropy production and lower variability in the

structural integrity (i.e., lower decreases in EVI; Fig. 1e). This suggests that the understory plays a crucial role in the structure and function of more open canopy ecosystems (Aoki, 2012; Lin, 2015), in addition to more productive overstory trees during summer. This led to similar entropy export efficiencies at all sites as evidenced by all sites having comparable dS/dt. Nevertheless, as σ increased with greater absorption of radiation due to an increase in EVI, J_H decreased as a result of higher SWC, resulting in temporary entropy accumulation at the xeric site during the end of 2012 (SI Fig. 4), which may have contributed to higher T_{air} compared to the other sites (Fig. 2).

In contrast, the mesic site was affected by the interaction of biological and radiative forces, as J_{LE} and eff_{rad} decreased more severely with decreasing plant leaf area compared to the xeric site (lower EVI; Fig. 1e). As a consequence of lower LE and J_{LE} during the drought, more energy was partitioned into H in 2011 (Fig. 6), as air, soil and surface temperatures increased due to lower leaf area (Figs. 1 and 2), indicating a shift of ecosystem function (Ban-Weiss et al., 2011) towards lower quality energy degradation (Kuricheva et al., 2017). This initially depleted soil moisture storage at the mesic site (Fig. 1) and further decreased LE and J_{LE} (Kim and Wang, 2012; Lauri et al., 2014). Nevertheless, the shift in energy partitioning at the mesic site allowed for the maintenance of dS/dt during drought, by export of entropy which had accumulated during nighttime hours (SI Fig. S4), demonstrating an adaptation of the site to changes in resource availability (Basu et al., 2016; Brodribb et al., 2014). In contrast, the xeric and intermediate sites showed greater variability in annual dS/dt following the drought when rainfall returned to pre-drought levels and SWC increased (Fig. 10a). Nevertheless, the rapid increase in J_{LE} in 2012 at the mesic and xeric sites indicated an increase in ecosystem function through greater evapotranspiration. This provides evidence of recovery following the drought, because J_{LE} is of higher quality entropy dissipation (Kuricheva et al., 2017), coupling both mass and heat dynamics (Brunsell et al., 2011), whereas J_H is a function of the thermal gradient (Kleidon, 2010; LeMone et al., 2007). In general, plant species at the mesic site were better adapted to higher soil water conditions, as entropy and energy fluxes did not change as drastically with increasing SWC compared to the other sites.

This recovery of EVI following drought also allowed for greater eff_{rad} at the sites. But eff_{rad} was higher at the mesic site despite lower EVI compared to the intermediate site. This finding supports our second hypothesis, that sites with greater plant functional diversity maintain greater radiative entropy production. The mesic site efficiently used available energy from incoming solar radiation (Fig. 2) through lower reflection of R_s and by emitting less longwave radiation (Lin, 2015). Eff_{rad} decreased during the initial drought year because all sites reflected more R_s, likely a consequence of a change in EVI, as well as leaf angle from a decrease in SWC and altered plant hydraulics. Higher eff_{rad} and eff_{flux} at the mesic site are consistent with enhanced function due to greater plant diversity in the understory (Fig. 4a). For example, wiregrass, a C_4 species, can maintain photosynthetic rates under high temperatures (Osborne and Sack, 2012; Ward et al., 1999), which allows for greater energy storage during unfavorable environmental conditions (Brunsell et al., 2011). Despite higher wiregrass biomass in the understory, the xeric site was less efficient in using available radiation energy, indicated by high $R_{s,out}$ and $R_{l,out}$ (Brunsell et al., 2011). Structural limitations of the canopy (i.e., lower basal area), impeded the efficient absorption of available radiation, therefore lowering eff_{rad} (Norris et al., 2011). Furthermore, larger proportions of deciduous oak trees at the xeric site (Table 1), which typically shed their leaves during the winter, lowered the capacity of the system to acquire radiation (Baldocchi et al., 2004: Fig. 8b). Nevertheless, this inefficiency was not confirmed by model results for S_m, which, in contrast to NEE_e

revealed higher metabolic function at the xeric site relative to the mesic and intermediate sites, reflecting greater metabolic performance despite differences in basal area and site EVI. Overall our results demonstrate that the mesic site was better adapted to changes in resource availability by way of altering its reflective properties, where energy partitioning adjusted to maintain steady entropy exports relative to incoming entropy (Gunawardena et al., 2017; Otto et al., 2014; Taha et al., 1988). Nevertheless, metabolic activity decreased during rainy periods ($S_m \sim 0$), demonstrating an inefficiency in maintaining optimal function when environmental pressure was imposed on the system. High metabolic function at the mesic site resulted in more rapid increases in the structural complexity as indicated by a decrease in $R_{s,out}$ following the drought when compared to the intermediate site (Brunsell et al., 2011; Holdaway et al., 2010). Metabolic activity (in energy terms) at the intermediate site was largely dependent on EVI (i.e., leaf area), demonstrating lower biological control of individual plant species (i.e., stomatal control; Urban et al. 2016), but a strong influence of total leaf area on metabolic function and the export of entropy (Brunsell et al., 2011; Fig. 4 and 6). This was further illustrated at the intermediate site through less negative metabolic energy (NEE_e) when EVI was ~ 0.25 (Fig. 7c). Even though EVI in 2012 was greater at the intermediate site this did not correspond to higher J_{LE} (Fig. 5a), which was also shown by a lack of significant change in entropy exports with changes in EVI (eff_{flux}, Fig. 9c). The result of lower metabolic function at the intermediate site is intriguing as the mesic and intermediate sites were structurally similar, based on similar B_A, mean DBH and overstory tree composition (Table 1). The inefficiency appears to be a consequence of anthropogenic modification, which homogenized the ecosystem, leading to a decrease in understory plant functional types (Table. 1; Fig. 3), thereby reducing values of eff_{rad}, eff_{flux} and S_m. This result provides evidence that the intermediate site was less efficient in absorbing energy and dissipating entropy compared to the mesic site, resulting in slower adaptation to drought. Similar results were shown in Lin et al. (2015), where disturbed sites had predominantly lower entropy production rates, as well as in Lin et al. (2018) where greater surface temperature led to decreased σ, which we also observed at the intermediate site. Our third hypothesis was therefore supported, as the intermediate site had lower eff_{flux} relative to the mesic and xeric sites. Lower plant functional diversity, specifically the lack of wiregrass, due to soil perturbations that took place prior to stand establishment (>95 years ago), likely lowered metabolic function, which in turn affected entropy exports at the intermediate site and its recovery from drought. For example, a negative J_G at the intermediate site was observed with increasing SWC suggesting poor soil water drainage, which is also likely a consequence of agricultural legacy (Kozlowski, 1999). A prolonged increase in eff_{flux} compared to the other sites showed that the intermediate site did not adapt its entropy exports, in addition to greater reflection of R_s during drought recovery. This result indicates that differences in soil conditions and lower plant functional diversity at the intermediate site reduced entropy exports compared to the other sites (Meysman and Bruers, 2010), such that plant functional types present at the site could not rescue the ecosystem's function during disturbance (Elmqvist et al., 2003). Furthermore, while the intermediate site showed no change in dS/dt during the drought, following the drought the export of entropy significantly increased, resulting in more unstable conditions (Fig. 10a). The increase in entropy export corresponded to high annual rainfall and soil moisture conditions (Figs. 1 and S1), once more suggesting that soil characteristics were altered due to its agricultural legacy. The lower ability to adapt to changes in resource availability at the intermediate site could induce its degradation if environmental fluctuations, become more frequent and severe with climate

change (Mori, 2011; Siteur et al., 2016). This could further exacerbate instabilities for nearby sites, as changes in the reflective properties of degraded sites can alter microclimate and weather patterns across whole ecosystems (Norris et al., 2011).

We conclude that the analysis of entropy dynamics, in relation to structural and environmental variables gives valuable insights into the functional complexity of ecosystems and their ability to adapt to drought. A combination of entropy fluxes and entropy ratios revealed how differences in structural and/or functional characteristics affect energy efficiencies in longleaf pine ecosystems. Our results show that all sites demonstrated adaptive capacity to extreme drought, as indicated by a lack of significant change in dS/dt, except for greater variations at the xeric and intermediate sites following the drought. We show that overall low entropy exports at the site with greater land use legacy had the potential to decrease ecosystem function (Meysman and Bruers, 2010), especially during high rainfall events. Changes in climate and natural and human induced disturbances are becoming more frequent and severe (IPCC, 2014), demanding more predictive power about how changes in ecosystem structure and function will alter resilience to disturbances. Future policy, conservation or restoration applications depend on reliable measures such as the metrics presented here, to monitor ecosystem function following disturbances (Haddeland et al., 2014; Porter et al., 2012; Reinmann and Hutyra, 2016; Thom et al., 2017). This is especially critical for anthropogenically modified systems, as their land use history can affect changes in energy use efficiency and thus alter their ability to recover from disturbances (Bürgi et al., 2016; Foster et al., 2003). The application of entropy metrics could improve our understanding of the interaction of structure, function and legacy on energy use efficiency across a variety of global ecosystems.

Author contribution

G.S. and L.B. designed and acquired funding for the research. S.W. and C.S. analyzed the data. P.S. aided S.W. with the theories of entropy and energy density. All authors contributed to writing of the manuscript.

Acknowledgement

The authors thank the Forest Ecology laboratories personnel, with special thanks to Tanner Warren, Andres Baron-Lopez and Scott Taylor, for data collection and provision during the study at the Joseph W. Jones Ecological Research Center. CS and GS acknowledge support from the U.S. National Science Foundation (DEB EF-1241881). PS acknowledges support from the U.S. National Science Foundation (DEB 1552976, and 1702029) and the USDA National Institute of Food and Agriculture (Hatch project 228396).

References

Amthor, J. S.: From sunlight to phytomass: On the potential efficiency of converting solar radiation to phyto-energy, New Phyt., 188(4), 939–959, doi:10.1111/j.1469-8137.2010.03505.x, 2010.

Aoki, I.: Entropy Principle in Living Systems (Min–Max Principle), Entropy Principle for the Development of Complex Biotic Systems, (Chapter 2), 87–88, doi:10.1016/B978-0-12-391493-4.00008-1, 2012.

Baldocchi, D. D., Xu, L. and Kiang, N.: How plant functional-type, weather, seasonal drought, and soil physical properties alter water and energy fluxes of an oak–grass savanna and an annual grassland, Agric. For. Meteorol., 123(1-2), 13–39, doi:10.1016/j.agrformet.2003.11.006, 2004.

Ban-Weiss, G. A., Bala, G., Cao, L., Pongratz, J. and Caldeira, K.: Climate forcing and response to idealized changes in surface latent and sensible heat, Environ. Res. Lett., 6(3), 034032, doi:10.1088/1748-9326/6/3/034032, 2011.

Basu, S., Ramegowda, V., Kumar, A. and Pereira, A.: Plant adaptation to drought stress, F1000Research, 5(0), 1554, doi:10.12688/f1000research.7678.1, 2016.

Beer, C., Ciais, P., Reichstein, M., Baldocchi, D., Law, B. E., Papale, D., Soussana, J. F., Ammann, C., Buchmann, N., Frank, D., Gianelle, D., Janssens, I. A., Knohl, A., Köstner, B., Moors, E., Roupsard, O., Verbeeck, H., Vesala, T., Williams, C. A. and Wohlfahrt, G.: Temporal and among-site variability of inherent water use efficiency at the ecosystem level, Global Biogeochem. Cycles, 23(2), n/a–n/a, doi:10.1029/2008GB003233, 2009.

Bohn, F. J. and Huth, A.: The importance of forest structure to biodiversity–productivity relationships, R. Soc. open sci., 4(1), 160521, doi:10.1098/rsos.160521, 2017.

Bonan, G. B.: Forests and climate change: forcings, feedbacks, and the climate benefits of forests. Science, 320(5882), 1444-1449, doi: 10.1126/science.1155121, 2008.

Brodribb, T. J., McAdam, S. A. M., Jordan, G. J. and Martins, S. C. V.: Conifer species adapt to low-rainfall climates by following one of two divergent pathways, Proc Natl Acad Sci USA, 111(40), 14489–14493, doi:10.1073/pnas.1407930111, 2014.

Brunsell, N. A., Schymanski, S. J. and Kleidon, A.: Quantifying the thermodynamic entropy budget of the land surface: Is this useful? Earth Sys. Dyn., 2(1), 87–103, 2011.

Bürgi, M., Östlund, L. and Mladenoff, D. J.: Legacy effects of human land use: Ecosystems as time-lagged systems, Ecosystems, 20(1), 94–103, doi:10.1007/s10021-016-0051-6, 2016.

Campbell, G. S. and Norman, C. G.: An introduction to environmental biophysics, Springer Science & Business Media. 1998.

Clement, R.: EdiRe data software, School of Geosciences, The University of Edinburgh, Edinburgh, Scotland. 1999.

DAAC, O.: MODIS collection 5 land products global subsetting and visualization tool: MOD13Q1 MODIS/Terra and MYD13Q1 MODIS/Aqua Vegetation Indices, NASA EOSDIS Land Processes DAAC, USGS Earth Resources Observation and Science EROS Center, 2008.

Dai, A., Qian, T., Dai, A., Trenberth, K. E. and Qian, T.: A Global Dataset of Palmer Drought Severity Index for 1870–2002: Relationship with Soil Moisture and Effects of Surface Warming, http://dx.doi.org/10.1175/JHM-386.1, 5(6), 1117–1130, doi:10.1175/JHM-386.1, 2004.

Elmqvist, T., Folke, C., Nyström, M., Peterson, G., Bengtsson, J., Walker, B. and Norberg, J.: Response diversity, ecosystem change, and resilience, Front. Ecol. Environ., 1(9), 488–494, doi:10.1890/1540-9295(2003)001[0488:RDECAR]2.0.CO;2, 2003.

Finzi, A. C., Norby, R. J., Calfapietra, C., Gallet-Budynek, A., Gielen, B., Holmes, W. E., Hoosbeek, M. R., Iversen, C. M., Jackson, R. B., Kubiske, M. E., Ledford, J., Liberloo, M., Oren, R., Polle, A., Pritchard, S., Zak, D. R., Schlesinger, W. H. and Ceulemans, R.: Increases in nitrogen uptake rather than nitrogen-use efficiency support higher rates of temperate forest productivity under elevated CO_2, Proc Natl Acad Sci USA, 104(35), 14014–14019, doi:10.1073/pnas.0706518104, 2007.

Foster, D., Swanson, F., Aber, J., Burke, I., Brokaw, N., Tilman, D. and Knapp, A.: The importance of land-use legacies to ecology and conservation, BioScience, 53(1), 77–88, doi:10.1641/0006-3568(2003)053[0077:TIOLUL]2.0.CO;2, 2003.

Fox, J. and Weisberg, S.: car: Companion to Applied Regression, Second Edition. Thousand Oaks CA, 2011.

Franklin, J., Serra-Diaz, J. M., Syphard, A. D. and Regan, H. M.: Global change and terrestrial plant community dynamics, Proc Natl Acad Sci USA, 113(14), 3725–3734, doi:10.1073/pnas.1519911113, 2016.

Fraedrich, K. and Lunkeit, F.: Diagnosing the entropy budget of a climate model, Tellus A: Dynamic Meteorology and Oceanography, 60, 921–931, doi: 10.3402/tellusa.v60i5.15498, 2008.

Goebel, P. C., Palik, B. J., Kirkman, L. K. and West, L.: Field guide: landscape ecosystem types of Ichauway. Joseph W. Jones Ecological Research Center at Ichauway, Newton, Report number 97–1. 1997.

Goebel, P. C., Palik, B. J., Kirkman, L. K., Drew, M. B., West, L. and Pederson, D. C.: Forest ecosystems of a Lower Gulf Coastal Plain landscape: Multifactor classification and analysis, J. Torrey Bot. Soc., 128(1), 47, doi:10.2307/3088659, 2001.

Gunawardena, K. R., Wells, M. J. and Kershaw, T.: Utilising green and bluespace to mitigate urban heat island intensity, Science of the Total Environment, The, 584-585, 1040–1055, doi:10.1016/j.scitotenv.2017.01.158, 2017.

Haddeland, I., Heinke, J., Biemans, H., Eisner, S., Flörke, M., Hanasaki, N., Konzmann, M., Ludwig, F., Masaki, Y., Schewe, J., Stacke, T., Tessler, Z. D., Wada, Y. and Wisser, D.: Global water resources affected by human interventions and climate change, Proc Natl Acad Sci USA, 111(9), 3251–3256, doi:10.1073/pnas.1222475110, 2014.

Hammerle, A., Haslwanter, A., Tappeiner, U., Cernusca, A., & Wohlfahrt, G.: Leaf area controls on energy partitioning of a temperate mountain grassland. Biogeosciences, 5(2), doi: 10.5194/bg-5-421-2008, 2008.

Hardiman, B. S., Bohrer, G., Gough, C. M., Vogel, C. S. and Curtis, P. S.: The role of canopy structural complexity in wood net primary production of a maturing northern deciduous forest, Ecology, 92(9), 1818–1827, doi:10.1890/10-2192.1, 2011.

Holdaway, R. J., Sparrow, A. D. and Coomes, D. A.: Trends in entropy production during ecosystem development in the Amazon Basin, Philos T Roy Soc B, 1437–1447, doi:10.1098/rstb.2009.0298, 2010.

IPCC: Climate Change 2014: Synthesis Report. Contribution of Working Groups I, II and III to the Fifth Assessment Report of the Intergovernmental Panel on Climate Change, edited by Core Writing Team, R. K. Pachauri, and L. A. Meyer, IPCC, Geneva. 2014.

Juang, J.-Y., Katul, G., Siqueira, M., Stoy, P. and Novick, K.: Separating the effects of albedo from eco-physiological changes on surface temperature along a successional chronosequence in the southeastern United States, Geophys Res Lett, 34, 1–5, doi:10.1029/2007GL031296, 2007.

Kaimal, J. C. and Gaynor, J. E.: Another look at sonic thermometry, Boundary-Layer Meteorol, 56(4), 401–410, doi:10.1007/BF00119215, 1991.

Khanna, J., Medvigy, D., Fueglistaler, S., & Walko, R.: Regional dry-season climate changes due to three decades of Amazonian deforestation. Nature Climate Change, 7(3), 200, doi: 10.1038/nclimate3226, 2017.

Kim, Y. and Wang, G.: Soil moisture-vegetation-precipitation feedback over North America: Its sensitivity to soil moisture climatology, Journal of Geophysical Research Atmospheres, 117(17), 1–18, doi:10.1029/2012JD017584, 2012.

Kirkman, L. K., Giencke, L. M., Taylor, R. S., Boring, L. R., Staudhammer, C. L. and Mitchel, R. J.: Productivity and species richness in longleaf pine woodlands: Resource-disturbance influences across an edaphic gradient, Ecology, 97(9), 2259–2271, doi:10.1002/ecy.1456, 2016.

Kirkman, L. K., Mitchell, R. J., Helton, R. C. and Drew, M. B.: Productivity and species richness across an environmental gradient in a fire-dependent ecosystem, Am. J. Bot., 88(11), 2119–2128, 2001.

Kleidon, A., & Lorenz, R. D. (Eds.). Non-equilibrium thermodynamics and the production of entropy: life, earth, and beyond. Springer Science & Business Media, 2004.

Kleidon, A.: Nonequilibrium thermodynamics and maximum entropy production in the Earth system. Naturwissenschaften, 96(6), 1-25, https://doi.org/10.1007/s00114-009-0509-x, 2009.

Kleidon, A.: A basic introduction to the thermodynamics of the Earth system far from equilibrium and maximum entropy production, Philos T Roy Soc B, 365(1545), 1303–1315, doi:10.1098/rstb.2009.0310, 2010.

Kleidon, A., Malhi, Y. and Cox, P. M.: Maximum entropy production in environmental and ecological systems, Philos T Roy Soc B, 365(1545), 1297–1302, doi:10.1098/rstb.2010.0018, 2010.

Klein, T., Shpringer, I., Ben Fikler, Elbaz, G., Cohen, S. and Yakir, D.: Relationships between stomatal regulation, water-use, and water-use efficiency of two coexisting key Mediterranean tree species, For. Ecol. Manage., 302, 34–42, doi:10.1016/j.foreco.2013.03.044, 2013.

Kozlowski, T. T.: Soil compaction and growth of woody plants. Scandinavian Journal of Forest Research, 14(6), 596-619, doi.org/10.1080/02827589908540825, 1999.

Kuricheva, O., Mamkin, V., Sandlersky, R., Puzachenko, J., Varlagin, A. and Kurbatova, J.: Radiative entropy production along the paludification gradient in the southern taiga, Entropy, 19(1), 43, doi:10.3390/e19010043, 2017.

Lauri, P.-É., Marceron, A., Normand, F., Dambreville, A., Hortsys, U. P. R. and Island, R.: Soil water deficit decreases xylem conductance efficiency relative to leaf area and mass in the apple, The Journal of Plant Hydraulics, 1(Wery 2005), e0003, 2014.

LeMone, M. A., Chen, F., Alfieri, J. G., Tewari, M., Geerts, B., Miao, Q., Grossman, R. L. and Coulter, R. L.: Influence of land cover and soil moisture on the horizontal distribution of sensible and latent heat fluxes in southeast Kansas during IHOP_2002 and CASES-97, Journal of Hydrometeorology, 8(1), 68–87, doi:10.1175/JHM554.1, 2007.

Lenth, R. V.: Least-Squares Means: The R Package lsmeans, J. Stat. Soft., 69(1), doi:10.18637/jss.v069.i01, 2016.

Lin, H.: Thermodynamic entropy fluxes reflect ecosystem characteristics and succession, Ecol. Model., 298, 75–86, doi:10.1016/j.ecolmodel.2014.10.024, 2015.

Lin, H., Zhang, H., & Song, Q.: Transition from abstract thermodynamic concepts to perceivable ecological indicators. Ecological Indicators, 88, 37-42, doi: 10.1016/j.ecolind.2018.01.00, 2018.

Massmann, A., Gentine, P., & Lin, C.: When does vapor pressure deficit drive or reduce evapotranspiration?, arXiv preprint arXiv:1805.05444, doi: 10.5194/hess-2018-553, 2018.

Meysman, F. J. R. and Bruers, S.: Ecosystem functioning and maximum entropy production: a quantitative test of hypotheses, Philos T Roy Soc B, 365(1545), 1405–1416, doi:10.1098/rstb.2009.0300, 2010.

Mori, A. S.: Ecosystem management based on natural disturbances: Hierarchical context and non-equilibrium paradigm, Journal of Applied Ecology, 48(2), 280–292, doi:10.1111/j.1365-2664.2010.01956.x, 2011.

Müller, F. and Kroll, F.: Integrating ecosystem theories - Gradients and orientors as outcomes of self-organized processes, International Journal of Design and Nature and Ecodynamics, 6(4), 318–341, doi:10.2495/DNE-V6-N4-318-341, 2011.

NCDC: Monthly Station Normals of Temperature, Precipitation, and Heating and Cooling Degree Days 1981–2010, National Climatic Data center, Asheville, NC. 2011.

Nikolov, N. T., Massman, W. J. and Schoettle, A. W.: Coupling biochemical and biophysical processes at the leaf level: an equilibrium photosynthesis model for leaves of C_3 plants, Ecol. Model., 80(2-3), 205–235, doi:10.1016/0304-3800(94)00072-P, 1995.

Norris, C., Hobson, P. and Ibisch, P. L.: Microclimate and vegetation function as indicators of forest thermodynamic efficiency, Journal of Applied Ecology, 49(3), 562–570, doi:10.1111/j.1365-2664.2011.02084.x, 2011.

Odum, H. T.: Self-Organization, transformity, and information, Monthley Weather Review, 242(4882), 1132–1139, doi:10.1126/science.242.4882.1132, 1988.

Osborne, C. P. and Sack, L.: Evolution of C_4 plants: A new hypothesis for an interaction of CO_2 and water relations mediated by plant hydraulics, Philos T Roy Soc B, 367(1588), 583–600, doi:10.1098/rstb.2011.0261, 2012.

Otto, J., Berveiller, D., Bréon, F. M., Delpierre, N., Geppert, G., Granier, A., Jans, W., Knohl, A., Kuusk, A., Longdoz, B., Moors, E., Mund, M., Pinty, B., Schelhaas, M. J. and Luyssaert, S.: Forest summer albedo is sensitive to species and thinning: How should we account for this in Earth system models? Biogeosciences, 11(8), 2411–2427, doi:10.5194/bg-11-2411-2014, 2014.

Ozawa, H., Ohmura, A., Lorenz, R. D., & Pujol, T.: The second law of thermodynamics and the global climate system: A review of the maximum entropy production principle. Reviews of Geophysics, 41(4), doi: 10.1029/ 2002RG000113, 2003.

Pascale, S., Gregory, J. M., Ambaum, M. H., Tailleux, R., & Lucarini, V.: Vertical and horizontal processes in the global atmosphere and the maximum entropy production conjecture. Earth System Dynamics, 3(1), 19-32, https://doi.org/10.5194/esd-3-19-2012, 2012.

Peng, S., Schmid, B., Haase, J. and Niklaus, P. A.: Leaf area increases with species richness in young experimental stands of subtropical trees, Journal of Plant Ecology, 10(1), 128–135, doi:10.1093/jpe/rtw016, 2017.

Pinheiro, J., Bates, D., DebRoy, S. and Sarkar, D.: “nlme” Linear and Nonlinear Mixed Effects Models, 3rd ed., 2014.

Porter, E. M., Bowman, W. D., Clark, C. M., Compton, J. E., Pardo, L. H. and Soong, J. L.: Interactive effects of anthropogenic nitrogen enrichment and climate change on terrestrial and aquatic biodiversity, Biogeochemistry, 114(1-3), 93–120, doi:10.1007/s10533-012-9803-3, 2012.

Reinmann, A. B. and Hutyra, L. R.: Edge effects enhance carbon uptake and its vulnerability to climate change in temperate broadleaf forests, Proc Natl Acad Sci USA, 114(1), 201612369–112, doi:10.1073/pnas.1612369114, 2016.

Renninger, H. J., Carlo, N. J., Clark, K. L. and Schäfer, K. V. R.: Resource use and efficiency, and stomatal responses to environmental drivers of oak and pine species in an Atlantic Coastal Plain forest, Front. Plant Sci., 6(103), 317, doi:10.3389/fpls.2015.00297, 2015.

Roman, D. T., Novick, K. A., Brzostek, E. R., Dragoni, D., Rahman, F. and Phillips, R. P.: The role of isohydric and anisohydric species in determining ecosystem-scale response to severe drought, Oecologia, 179(3), 641–654, doi:10.1007/s00442-015-3380-9, 2015.

Schymanski, S. J., Kleidon, A., Stieglitz, M., & Narula, J.: Maximum entropy production allows a simple representation of heterogeneity in semiarid ecosystems. Philosophical Transactions of the Royal Society of London B: Biological Sciences, 365(1545), 1449-1455, doi:10.1098/rstb.2009.0309, 2010.

Schneider, E. D. and Kay, J. J.: Complexity and thermodynamics. Towards a new ecology, Futures, 26(6), 626–647, doi:10.1016/0016-3287(94)90034-5, 1994.

Siteur, K., Eppinga, M. B., Doelman, A., Siero, E. and Rietkerk, M.: Ecosystems off track: rate-induced critical transitions in ecological models, Oikos, 125(12), 1689–1699, doi:10.1111/oik.03112, 2016.

Starr, G., Staudhammer, C. L., Wiesner, S., Kunwor, S., Loescher, H. W., Baron, A. F., Whelan, A., Mitchell, R. J. and Boring, L.: Carbon dynamics of *Pinus palustris* ecosystems following drought, Forests, 7(5), 98, doi:10.3390/f7050098, 2016.

Skene, K. R.: Life's a gas: A thermodynamic theory of biological evolution. Entropy, 17(8), 5522-5548, doi:10.3390/e17085522, 2015.

Stoy, P. C., Katul, G. G., Siqueira, M. B. S., Juang, J.-Y., Novick, K. A., McCarthy, H. R., C. Oishi, A., Uebelherr, J. M., Kim, H.-S. and Oren, R.: Separating the effects of climate and vegetation on evapotranspiration along a successional chronosequence in the southeastern US, Glob. Chang. Biol., 12(11), 2115–2135, doi:10.1111/j.1365-2486.2006.01244.x, 2006.

Stoy, P. C., Lin, H., Novick, K. A., Siqueira, M. B. S. and Juang, J.-Y.: The role of vegetation on the ecosystem radiative entropy budget and trends along ecological succession, Entropy, 16(7), 3710–3731, doi:10.3390/e16073710, 2014.

Taha, H., Akbari, H., Rosenfeld, A. and Huang, J.: Residential cooling loads and the urban heat island—the effects of albedo, Building and Environment, 23(4), 271–283, doi:10.1016/0360-1323(88)90033-9, 1988.

Thom, D., Rammer, W. and Seidl, R.: The impact of future forest dynamics on climate: interactive effects of changing vegetation and disturbance regimes, Ecol. Monogr., 87(4), 665–684, doi:10.1002/ecm.1272, 2017.

Thomas, R. T., Prentice, I. C., Graven, H., Ciais, P., Fisher, J. B., Hayes, D. J., Huang, M., Huntzinger, D. N., Ito, A., Jain, A., Mao, J., Michalak, A. M., Peng, S., Poulter, B., Ricciuto, D. M., Shi, X., Schwalm, C., Tian, H. and Zeng, N.: Increased light-use efficiency in northern terrestrial ecosystems indicated by CO_2 and greening observations, Geophysical Research Letters, 43(21), 11,339–11,349, doi:10.1002/2016GL070710, 2016.

Twine, T. E., Kustas, W. P., Norman, J. M., Cook, D. R., Houser, P. R., Meyers, T. P., Prueger, J. H. and Wesley, M. L.: Correcting eddy covariance flux underestimates over grassland, Agric. For. Meteorol., 103, 279–300, doi:10.1016/S0168-1923(00)00123-4, 2000.

Virgo, N. and Harvey, I.: Entropy Production in Ecosystems, in Advances in Artificial Life, vol. 4648, pp. 123–132, Springer, Berlin, Heidelberg. 2007.

Ward, J. K., Tissue, D. T., Thomas, R. B., and Strain, B. R.: Comparative responses of model C_3 and C_4 plants to drought in low and elevated CO_2, Glob. Chang. Biol., 5(8), 857–867, doi:10.1046/j.1365-2486.1999.00270.x, 1999.

Whelan, A., Mitchell, R., Staudhammer, C. and Starr, G.: Cyclic occurrence of fire and its role in carbon dynamics along an edaphic moisture gradient in longleaf pine ecosystems, edited by B. Bond-Lamberty, PLoS ONE, 8(1), e54045, doi:10.1371/journal.pone.0054045, 2013.

Woodward, G., Perkins, D. M. and Brown, L. E.: Climate change and freshwater ecosystems: impacts across multiple levels of organization, Philos T Roy Soc B, 365(1549), 2093–2106, doi:10.1098/rstb.2010.0055, 2010.

Wright, J. K., Williams, M., Starr, G., McGee, J., & Mitchell, R. J.: Measured and modelled leaf and stand-scale productivity across a soil moisture gradient and a severe drought. Plant, cell & environment, 36(2), 467-483, DOI: 10.1111/j.1365-3040.2012.02590.x, 2012.

Wu, W., & Liu, Y.: Radiation entropy flux and entropy production of the Earth system. Reviews of Geophysics, 48(2), doi: 10.1029/2008RG000275, 2010.

Zhu, J., Jiang, L. and Zhang, Y.: Relationships between functional diversity and aboveground biomass production in the Northern Tibetan alpine grasslands, Sci. Rep., 6(March), 1–8, doi:10.1038/srep34105, 2016.

Table 1: Stand characteristics at the mesic, intermediate and xeric sites at the Joseph W. Jones Ecological Research Center, Newton, GA, USA.

Characteristic	Mesic	Intermediate	Xeric
Mean DBH (cm)	25.9	42.5	22.5
B_A *P. palustris* (m^2 ha^{-1})	17.7	14.6	8.9
B_A all tree spp. (m^2 ha^{-1})	19.0	15.7	11.0
Proportion of oak overstory trees (%)	6.8	7.0	19.1
LAI (m^{-2} m^{-2})	1.0[a]	unknown	0.69[a]
Wiregrass in the understory (%)	28	5	24
Woody species in the understory (%)	12	15	10
Prescribed fire	Early spring of 2009, 2011, 2013, 2015	Early spring of 2009, 2011, 2013, 2015	Early spring of 2009, 2011, 2013, 2015

a Wright et al. 2012

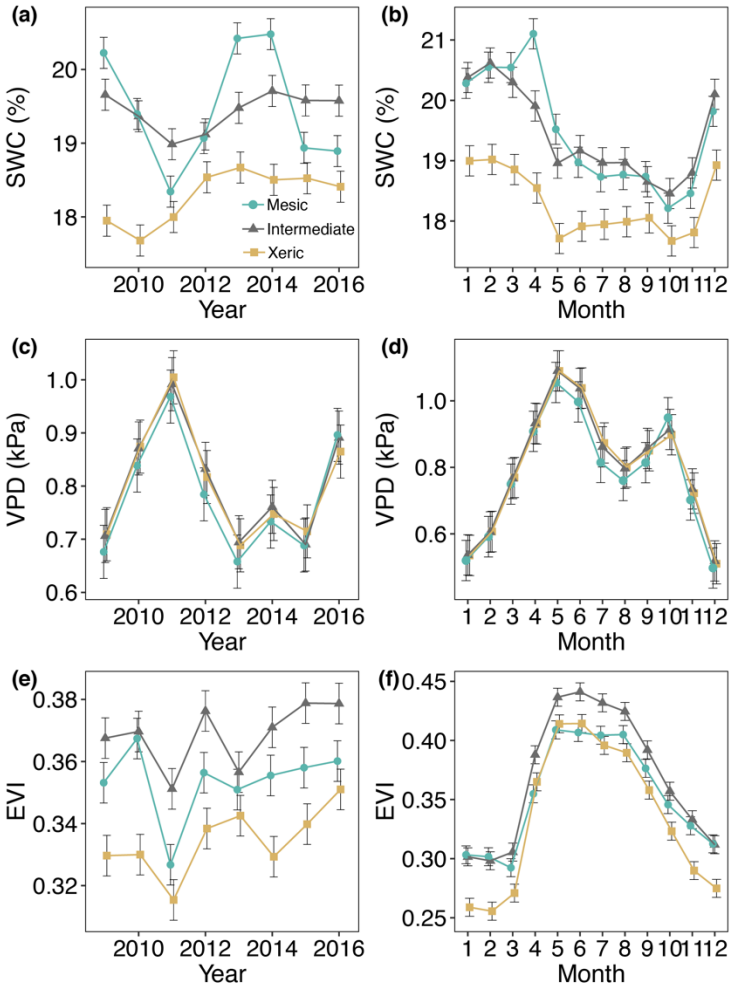

Figure 1: Least square mean predicted values from mixed models of environmental and structural variables for the years 2009-2016 at the mesic, intermediate and xeric sites, with average annual (a, c, and e) and monthly (b, d, and f) means of (a and b) soil water content (SWC), (c and d) vapor pressure deficit (VPD), and (e and f) enhanced vegetation index (EVI). Error bars represent standard errors (SE).

5

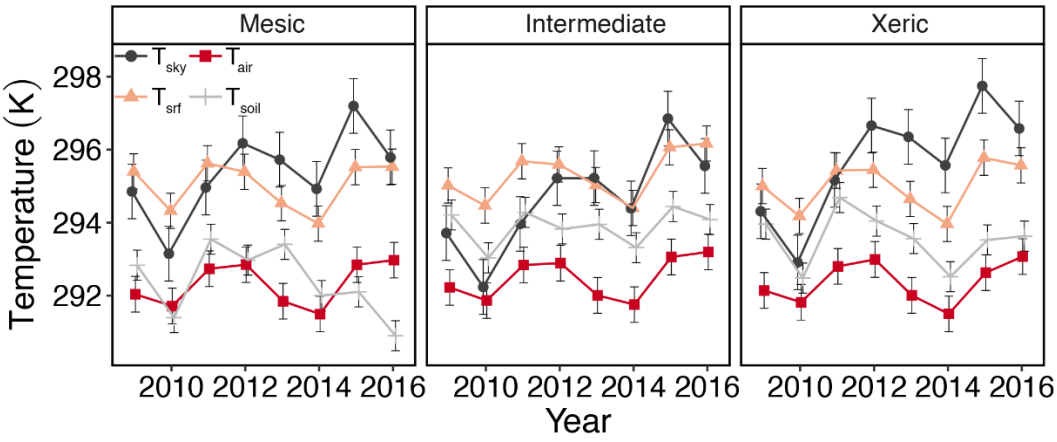

Figure 2: Least square mean predicted values from mixed models of annual sky temperature (T_{sky}), air temperature (T_{air}), surface temperature (T_{srf}), and soil temperature (T_{soil}) at the mesic, intermediate and xeric sites. Error bars represent SE.

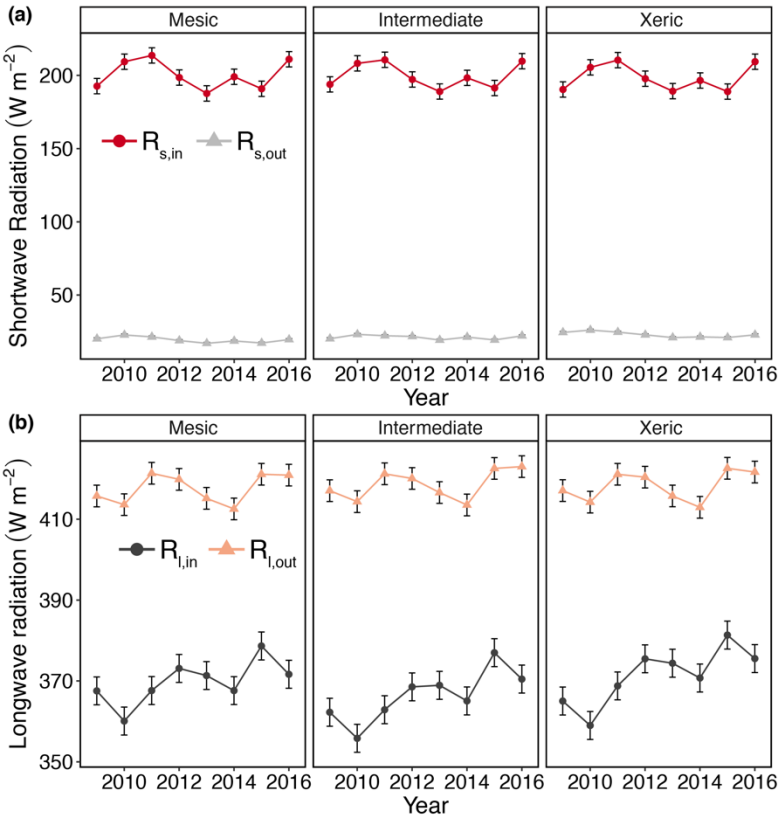

Figure 3: Least square mean predicted values from mixed models of annual average radiation at the mesic, intermediate and xeric sites for the years 2009-2016: (a) annual incoming and outgoing shortwave radiation ($R_{s,in}$ and $R_{s,out}$), and (b) annual incoming and outgoing longwave radiation ($R_{l,in}$ and $R_{l,out}$). Error bars represent SE.

5

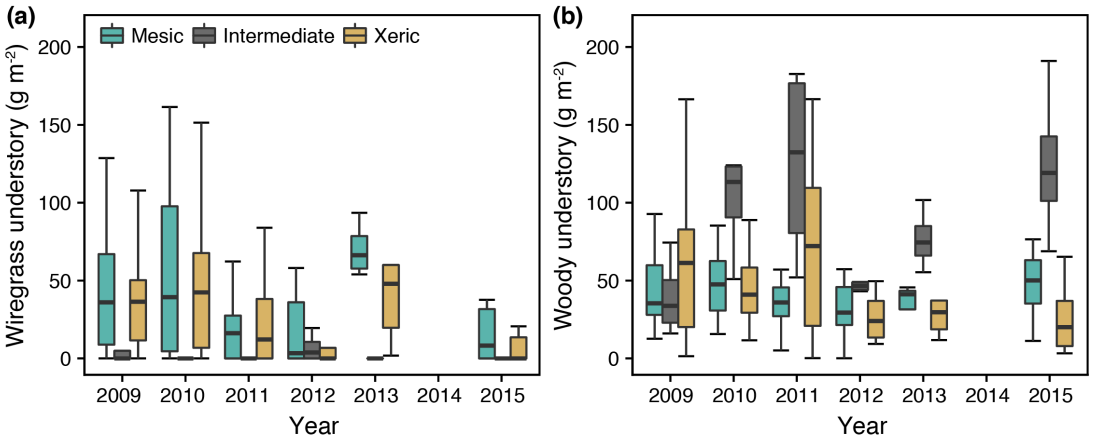

Figure 4: (a) Wiregrass and (b) woody understory biomass from 2009 through 2015 at the mesic, intermediate and xeric sites. Note that the sampling protocol changed to a 2-year measurements cycle in 2013, such that measurements were not made in 2014 and 2016.

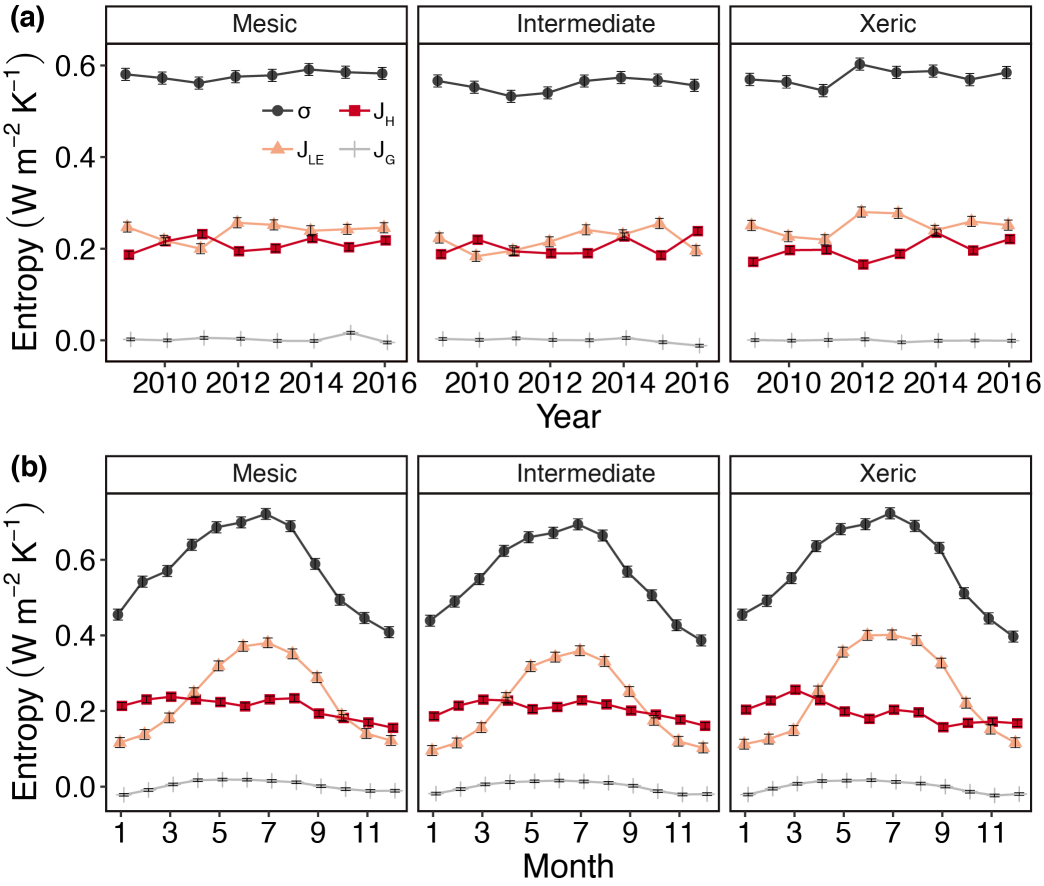

Figure 5: Least square mean predicted values from mixed models of annual (a) and monthly (b) average entropy production (σ) and entropy fluxes of latent energy (J_{LE}), sensible heat (J_H), and ground heat (J_G) at the mesic, intermediate and xeric sites. Error bars represent SE.

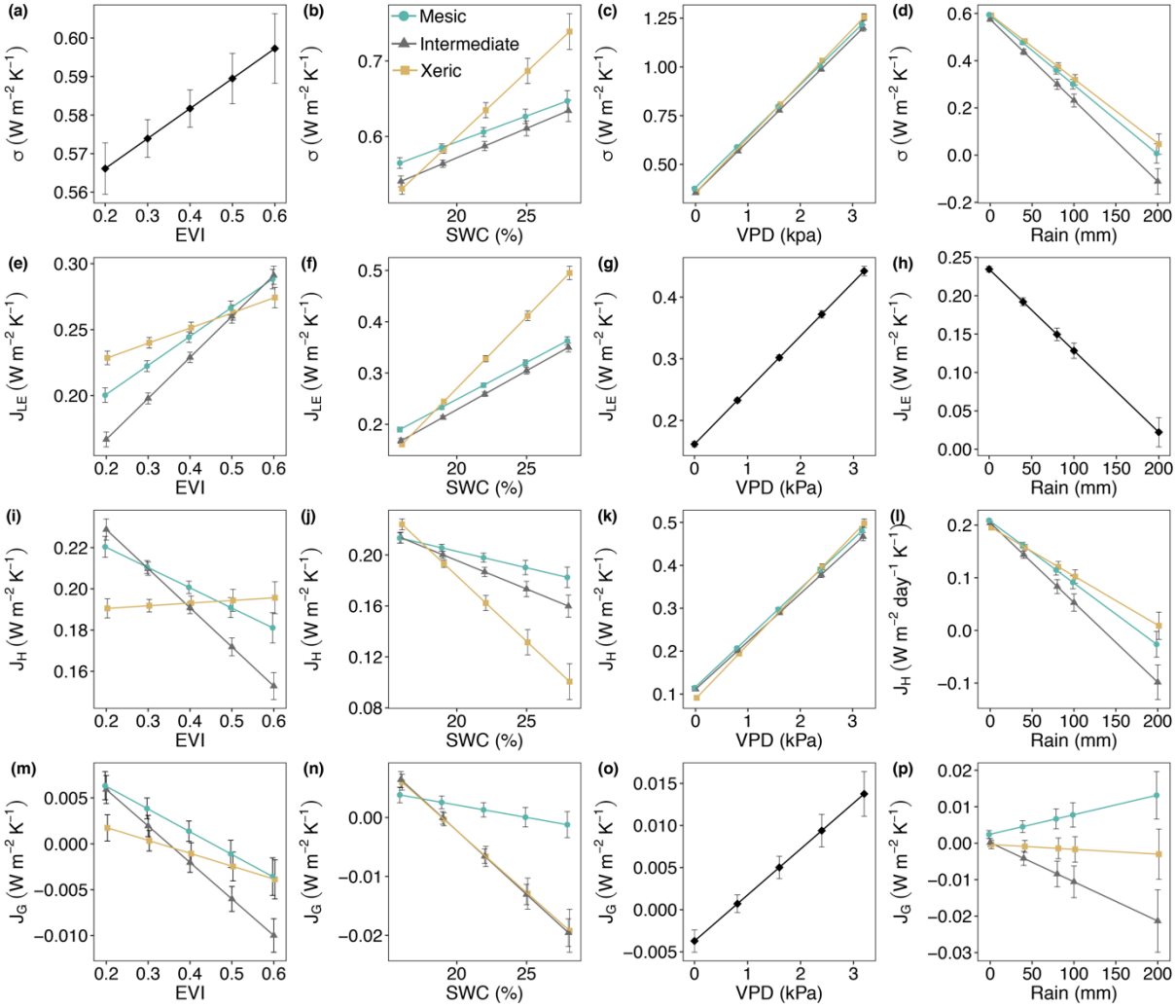

Figure 6: Least square mean predicted values from mixed models of (a-d) entropy production (σ) and entropy fluxes of (e-h) latent energy (J_{LE}), (i-l) sensible heat (J_H), and (m-p) ground heat (J_G) by site and (a, e, i, m) enhanced vegetation index (EVI), (b, f, j, n) soil water content (SWC), (c, g, k, o) vapor pressure deficit (VPD), and (d, h, l, p) rain. For (g), (h) and (o) the interaction with site was not significant, as signified by a single black line. Error bars represent SE.

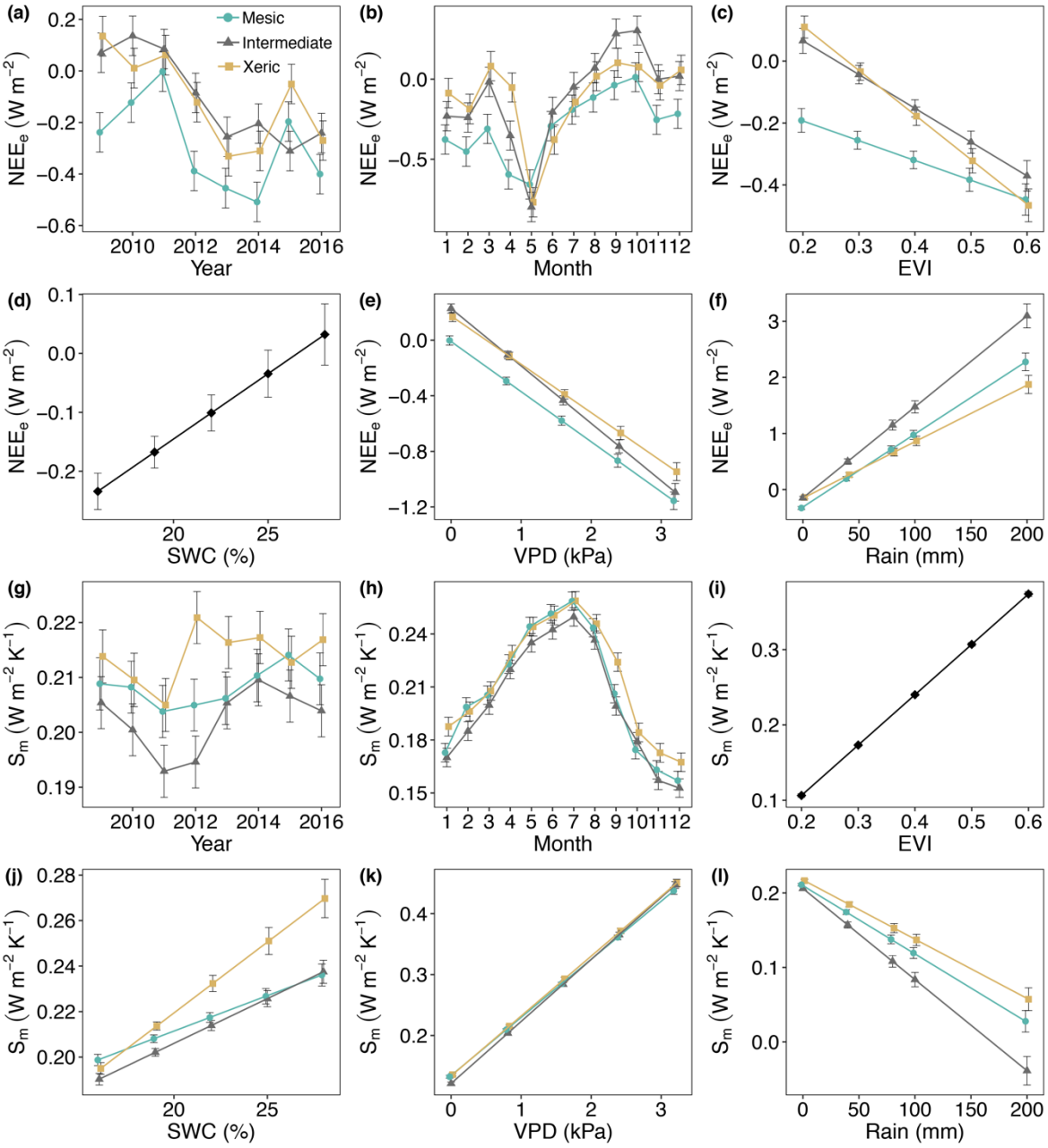

Figure 7: Least square mean predictive values from mixed model of (a-f) the metabolic energy flux (NEE_e) and (g and l) metabolic entropy fluxes of (S_m) by site and (a and g) year, (b and h) month, (c and i) enhanced vegetation index (EVI), (d and j) soil water content (SWC), (e and k) vapor pressure deficit (VPD), and (f and l) rain. For (d) and (i) the interaction with site was not significant, as indicated by a single solid black line. Error bars represent SE.

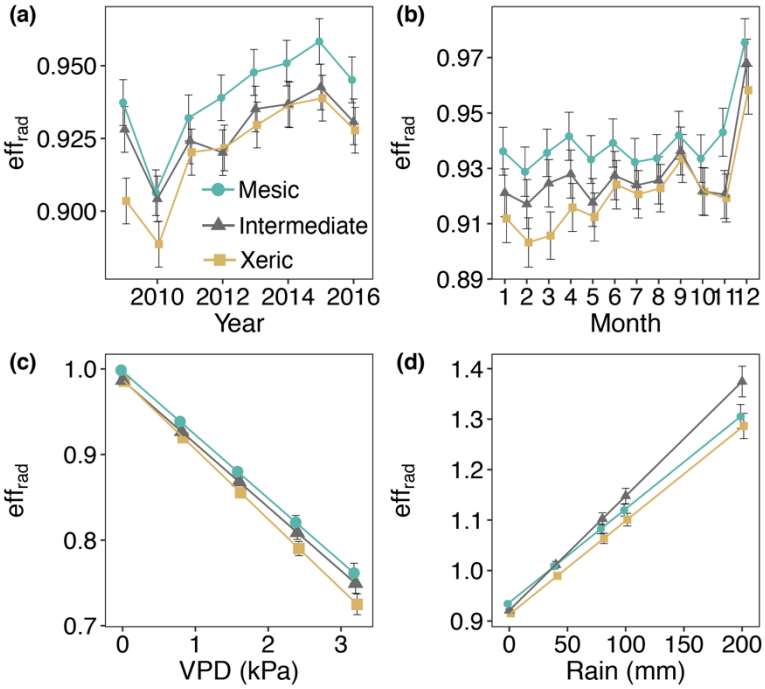

Figure 8: Least square mean predicted values from mixed models of average daily half-hourly radiative entropy efficiencies (eff_{rad}) at the mesic, intermediate and xeric sites by (a) year, (b) month, (c) vapor pressure deficit (VPD), and (d) rain. Soil water content and the enhanced vegetation index were not significant in the model. Error bars represent SE.

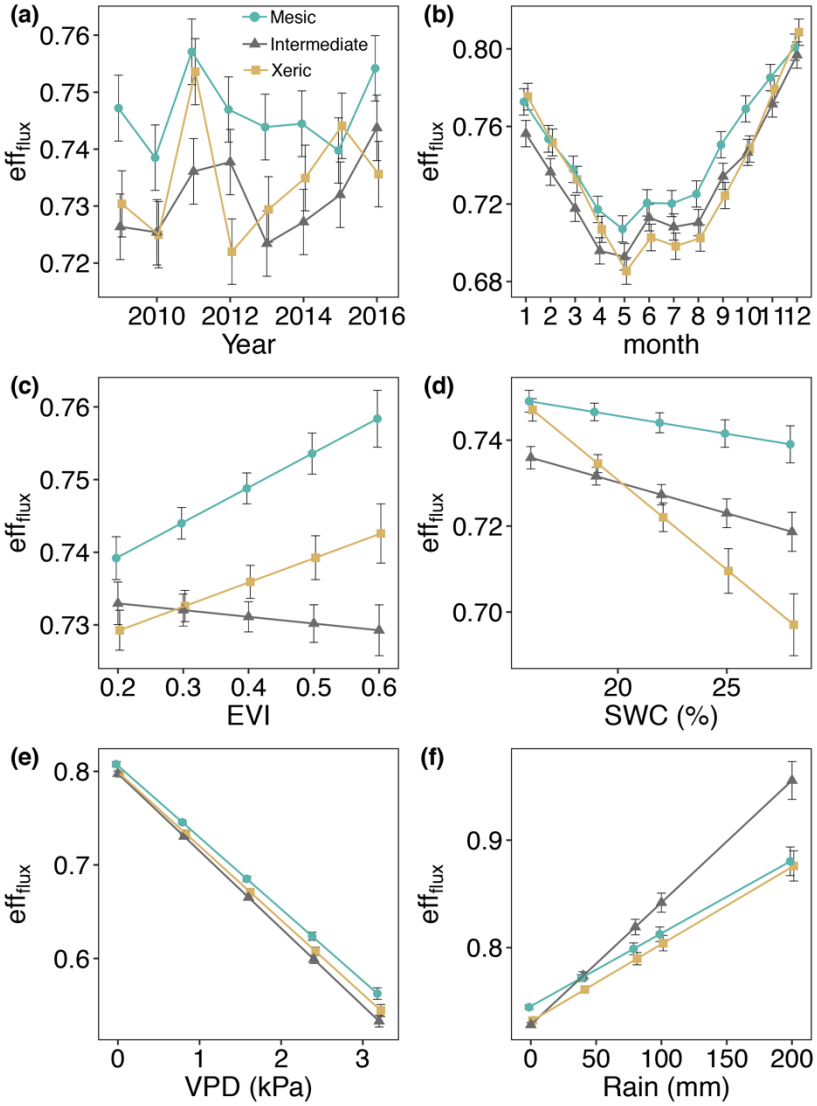

Figure 9: Least square mean predicted values from mixed models of average daily half-hourly flux entropy efficiencies (eff_{flux}) at the mesic, intermediate and xeric sites by (a) year, (b) month, (c) enhanced vegetation index (EVI), (d) soil water content (SWC), (e) vapor pressure deficit (VPD, and (f) rain. Error bars represent SE.

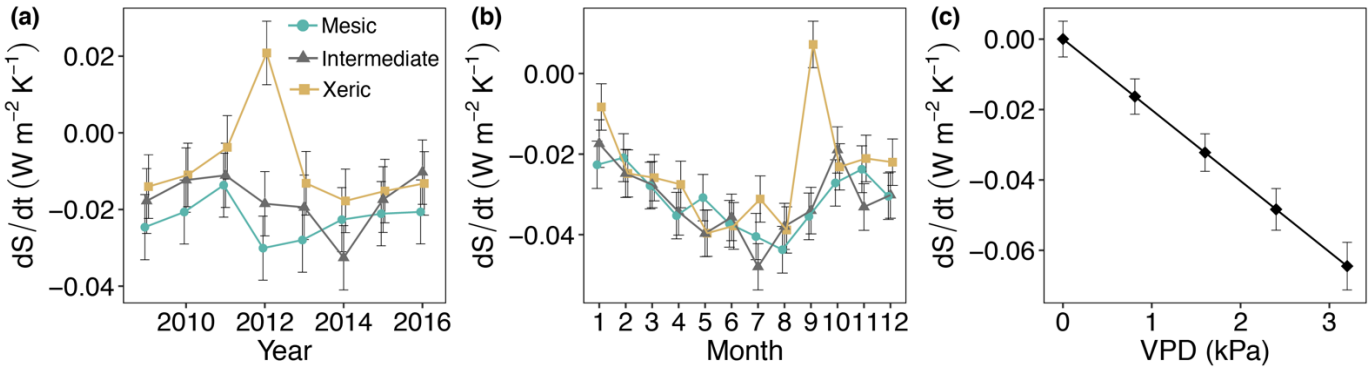

Figure 10: Least square mean predicted values from mixed models of average daily entropy at the mesic, intermediate and xeric sites by (a) year (a) month, (c) vapor pressure deficit (VPD). Soil water content and rain, as well as the interactions with site were not significant in the model. Error bars represent SE.

5

"Quantifying energy use efficiency via entropy production: A case study from longleaf pine ecosystems"

Table S1: Type 3 tests of fixed effects for model of rain.

Effect	Sum Sq.	Df	F value	Pr(>F)
Site	30607	2	4.2059	0.0159
Year	95938	7	3.7667	< 0.001

Table S2: Type 3 tests of fixed effects for the models of environmental variables and radiation.

Model	Effect	Chisq	Df	p-value
SWC	Site	6561.692	2	< 0.001
	Year	23.764	7	0.0013
	Month	94.089	11	< 0.001
	Site:Year	2629.617	14	< 0.001
	Site:Month	1398.986	22	< 0.001
VPD	Site	245.268	2	< 0.001
	Year	33.981	7	< 0.001
	Month	100.044	11	< 0.001
	Site:Year	214.101	14	< 0.001
	Site:Month	232.327	22	< 0.001
EVI	Site	2510.727	2	< 0.001
	Year	15.868	7	0.0264
	Month	597.701	11	< 0.001
	Site:Year	294.805	14	< 0.001
	Site:Month	791.727	22	< 0.001
T_{sky}	Site	2202.369	2	< 0.001
	Year	23.089	7	0.0017
	Month	912.141	11	< 0.001
	Site:Year	440.318	14	< 0.001
	Site:Month	63.082	22	< 0.001
T_{srf}	Site	438.625	2	< 0.001
	Year	12.844	7	0.076
	Month	1423.846	11	< 0.001
	Site:Year	435.639	14	< 0.001
	Site:Month	778.064	22	< 0.001
T_{air}	Site	1419.775	2	< 0.001
	Year	9.954	7	0.1912
	Month	1231.11	11	< 0.001
	Site:Year	1311.82	14	< 0.001
	Site:Month	336.866	22	< 0.001
T_{soil}	Site	5110.24	2	< 0.001
	Year	16.817	7	0.0186
	Month	1901.818	11	< 0.001
	Site:Year	1922.717	14	< 0.001
	Site:Month	5270.008	22	< 0.001
$R_{s,in}$	Site	0.9664	2	0.6168
	Year	16.3199	7	0.0224
	Month	763.0665	11	< 0.001
	Site:Year	121.9389	14	< 0.001
	Site:Month	170.75	22	< 0.001
$R_{s,out}$	Site	4161.151	2	< 0.001
	Year	48.782	7	< 0.001
	Month	682.874	11	< 0.001
	Site:Year	816.733	14	< 0.001
	Site:Month	1780.397	22	< 0.001
$R_{l,in}$	Site	2479.339	2	< 0.001
	Year	22.578	7	0.0020
	Month	1005.462	11	< 0.001
	Site:Year	482.99	14	< 0.001
	Site:Month	72.965	22	< 0.001
$R_{l,out}$	Site	226.43	2	< 0.001
	Year	13.07	7	0.0704
	Month	1433.87	11	< 0.001
	Site:Year	137.39	14	< 0.001
	Site:Month	980.18	22	< 0.001

Table S3: Type 3 tests of fixed effects for the models of energy.

Model	Effect	Chisq.	Df	Pr(>Chisq)
R_n	Year	20.6658	7	0.0042975
	Month	1927.222	11	< 0.001
	SWC	58.6889	1	< 0.001
	Site	650.5143	2	< 0.001
	EVI	12.2151	1	0.0005
	Rain	140.9816	1	< 0.001
	VPD	1756.8922	1	< 0.001
	Month:Site	120.9114	22	< 0.001
	SWC:Site	24.2945	2	< 0.001
	Site:EVI	7.3321	2	0.0256
	Site:VPD	16.6743	2	0.0002
	Year:Site	263.8642	14	< 0.001
LE	Year	20.7768	7	0.0041
	Month	754.2793	11	< 0.001
	SWC	455.4372	1	< 0.001
	Site	476.4295	2	< 0.001
	EVI	149.9341	1	< 0.001
	Rain	116.5615	1	< 0.001
	VPD	1043.0314	1	< 0.001
	Month:Site	369.8495	22	< 0.001
	SWC:Site	130.9093	2	< 0.001
	Site:EVI	43.0759	2	< 0.001
	Site:VPD	5.3897	2	0.0676
	Year:Site	564.6937	14	< 0.001
H	Year	39.525	7	< 0.001
	Month	108.742	11	< 0.001
	SWC	29.086	1	< 0.001
	Site	90.131	2	< 0.001
	EVI	25.974	1	< 0.001
	Rain	95.918	1	< 0.001
	VPD	1320.893	1	< 0.001
	Month:Site	301.757	22	< 0.001
	SWC:Site	35.234	2	< 0.001
	Site:EVI	41.862	2	< 0.001
	Site:VPD	29.24	2	< 0.001
	Site:Rain	16.416	2	0.0003
	Year:Site	351.685	14	< 0.001
G	Year	9.1742	7	0.2404
	Month	180.4785	11	< 0.001
	SWC	37.8658	1	< 0.001
	Site	200.7208	2	< 0.001
	EVI	33.4003	1	< 0.001
	Rain	0.1512	1	0.6974
	VPD	36.7781	1	< 0.001
	Month:Site	375.8069	22	< 0.001
	SWC:Site	38.7949	2	< 0.001
	Site:EVI	8.2576	2	0.0161
	Site:Rain	14.6424	2	0.0007
	Site:VPD	6.4624	2	0.0395
	Year:Site	990.9702	14	< 0.001

Table S4: Type 3 tests of fixed effects for models of entropy.

Model	Effect	Chisq	Df	Pr(>Chisq)
σ	Year	4.8186	7	0.6821
	Month	615.1107	11	< 0.001
	SWC	37.0574	1	< 0.001
	Site	146.6553	2	< 0.001
	EVI	6.1264	1	0.0133
	Rain	247.8162	1	< 0.001
	VPD	2170.749	1	< 0.001
	Month:Site	156.0447	22	< 0.001
	SWC:Site	22.0878	2	< 0.001
	Site:VPD	10.2957	2	0.0058
	Site:Rain	9.0465	2	0.0109
	Year:Site	117.8733	14	< 0.001
J_{LE}	Year	21.216	7	0.0035
	Month	726.81	11	< 0.001
	SWC	456.76	1	< 0.001
	Site	493.661	2	< 0.001
	EVI	148.839	1	< 0.001
	Rain	127.775	1	< 0.001
	VPD	1011.278	1	< 0.001
	Month:Site	367.42	22	< 0.001
	SWC:Site	162.581	2	< 0.001
	Site:EVI	42.076	2	< 0.001
	Year:Site	560.321	14	< 0.001
J_H	Year	38.625	7	< 0.001
	Month	101.071	11	< 0.001
	SWC	25.483	1	< 0.001
	Site	93.504	2	< 0.001
	EVI	25.804	1	< 0.001
	Rain	94.524	1	< 0.001
	VPD	1208.397	1	< 0.001
	Month:Site	315.446	22	< 0.001
	SWC:Site	39.127	2	< 0.001
	Site:EVI	44.953	2	< 0.001
	Site:VPD	30.372	2	< 0.001
	Site:rRain	14.251	2	0.0008
	Year:Site	370.91	14	< 0.001
J_G	Year	7.6197	7	0.3673
	Month	180.1628	11	< 0.001
	SWC	35.1066	1	< 0.001
	Site	234.691	2	< 0.001
	EVI	31.1994	1	< 0.001
	Rain	0.8563	1	0.3548
	VPD	29.1953	1	< 0.001
	Month:Site	299.2461	22	< 0.001
	SWC:Site	56.2234	2	< 0.001
	Site:EVI	11.0306	2	0.004
	Site:Rain	22.1752	2	< 0.001
	Year:Site	1082.405	14	< 0.001

Table S5: Type 3 tests of fixed effects for models of metabolic energy (NEE_e) and entropy (S_m).

Effect	Chisq	Df	Pr(>Chisq)	Effect
NEE_e	Year	29.646	7	0.0001102
	Month	74.127	11	< 0.001
	SWC	19.826	1	< 0.001
	Site	779.838	2	< 0.001
	EVI	75.114	1	< 0.001
	Rain	300.884	1	< 0.001
	VPD	327.07	1	< 0.001
	Month:Site	742.229	22	< 0.001
	Site:EVI	14.519	2	0.0007
	Site:VPD	11.067	2	0.0034
	Site:Rain	42.48	2	< 0.001
	Year:Site	520.107	14	< 0.001
S_m	Year	4.1562	7	0.7616
	Month	475.1864	11	< 0.001
	SWC	63.6594	1	< 0.001
	Site	138.5192	2	< 0.001
	EVI	3580.1388	1	< 0.001
	Rain	189.1466	1	< 0.001
	VPD	2433.3156	1	< 0.001
	Month:Site	129.5421	22	< 0.001
	SWC:Site	13.7285	2	0.001
	Site:VPD	12.6944	2	0.0002
	Site:Rain	26.3357	2	< 0.001
	Year:Site	118.2567	14	< 0.001

Table S6: Type 3 tests of fixed effects for models of entropy efficiency.

Model	Effect	Chisq	Df	Pr(>Chisq)
$\mathbf{eff_{rad}}$	Site	351.3632	2	< 0.001
	Year	26.8439	7	0.0004
	Month	26.4847	11	0.0055
	VPD	282.0899	1	< 0.001
	Rain	282.8825	1	< 0.001
	Site:Month	74.9708	22	< 0.001
	Site:VPD	9.8219	2	0.0074
	Site:Rain	17.4162	2	0.0001
	Site:Year	121.4967	14	< 0.001
$\mathbf{eff_{flux}}$	Mite	938.8639	2	< 0.001
	Year	9.2791	7	0.2332
	Month	251.1215	11	< 0.001
	VPD	1204.1726	1	< 0.001
	EVI	5.4535	1	0.0195
	Rain	122.5276	1	< 0.001
	SWC	8.9111	1	0.0028
	Site:Month	307.582	22	< 0.001
	Site:SWC	25.8864	2	< 0.001
	Site:VPD	17.4305	2	0.0002
	Site:Rain	51.4031	2	< 0.001
	Site:EVI	15.1919	2	0.0005
	Site:Year	517.3889	14	< 0.001
dS/dt	Site	31.8302	2	< 0.001
	Year	5.4413	7	0.6063
	Month	30.5512	11	0.0013
	VPD	139.6233	1	< 0.001
	Site:Month	100.2884	22	< 0.001
	Site:Year	124.8501	14	< 0.001

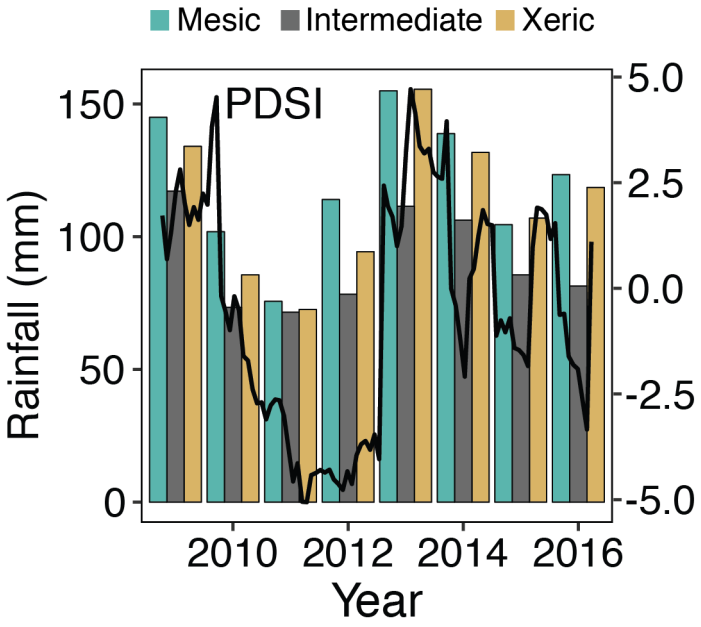

Figure S1: Monthly rainfall sums and Palmer Drought Severity Index (PDSI) for the mesic, intermediate and xeric sites from 2009 through 2016.

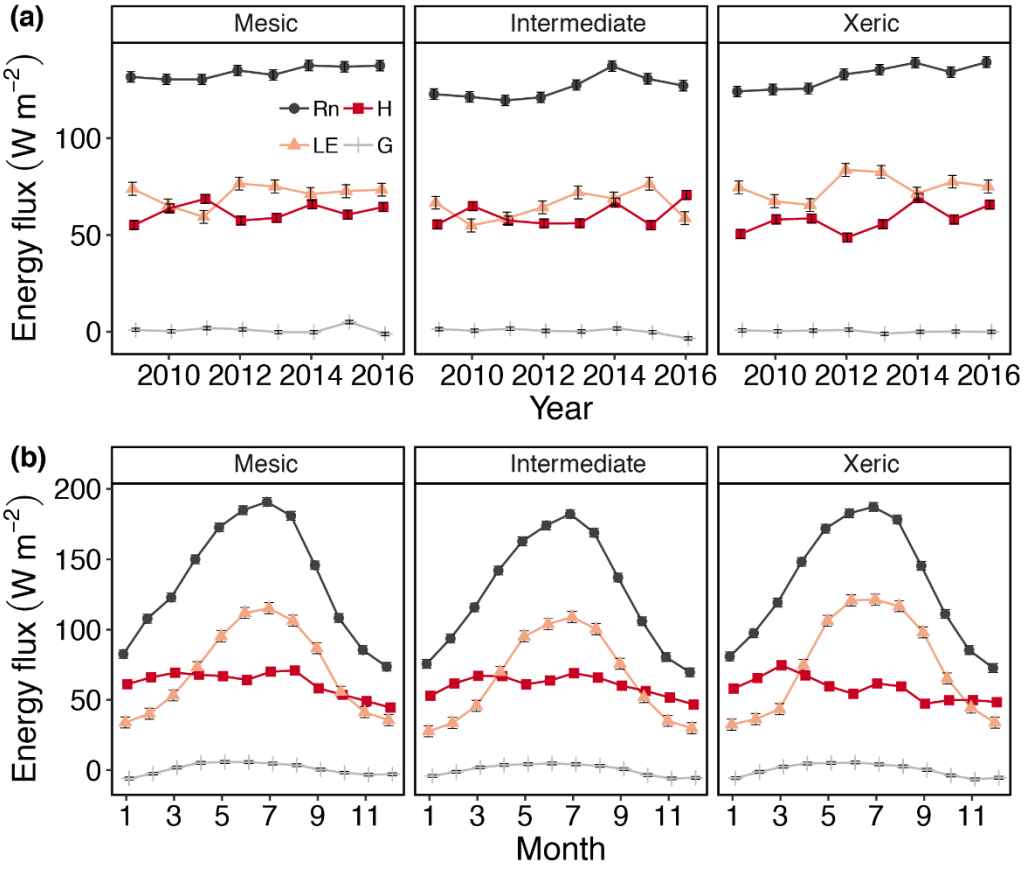

Figure S2: Annual (a) and monthly (b) changes of the energy fluxes of net radiation (R_n), latent energy (LE), sensible heat (H), and ground heat (G) at the mesic, intermediate and xeric sites.

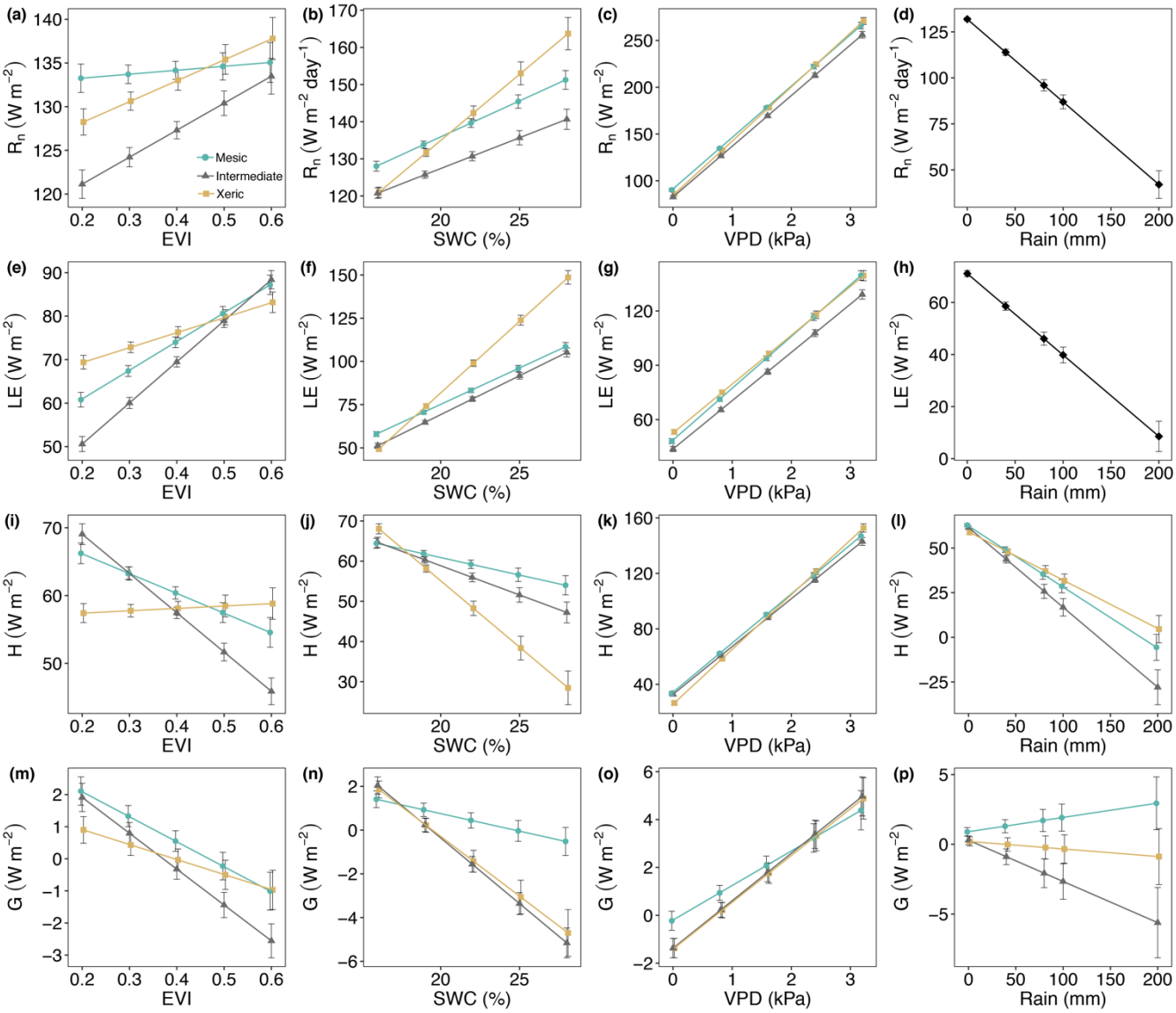

Figure S3: Least square mean predicted values from mixed models of energy fluxes of (a-d) net radiation (R_n), (e-h) latent energy (LE), (i-l) sensible heat (H), and (m-p) ground heat (G) by site and (a, e, i, m) enhanced vegetation index (EVI), (b, f, j, n) soil water content (SWC), (c, g, k, o) vapor pressure deficit (VPD) and (d, h, l, p) rain. For (d) and (h) the interaction with site was not significant, as indicated by a single solid black line.

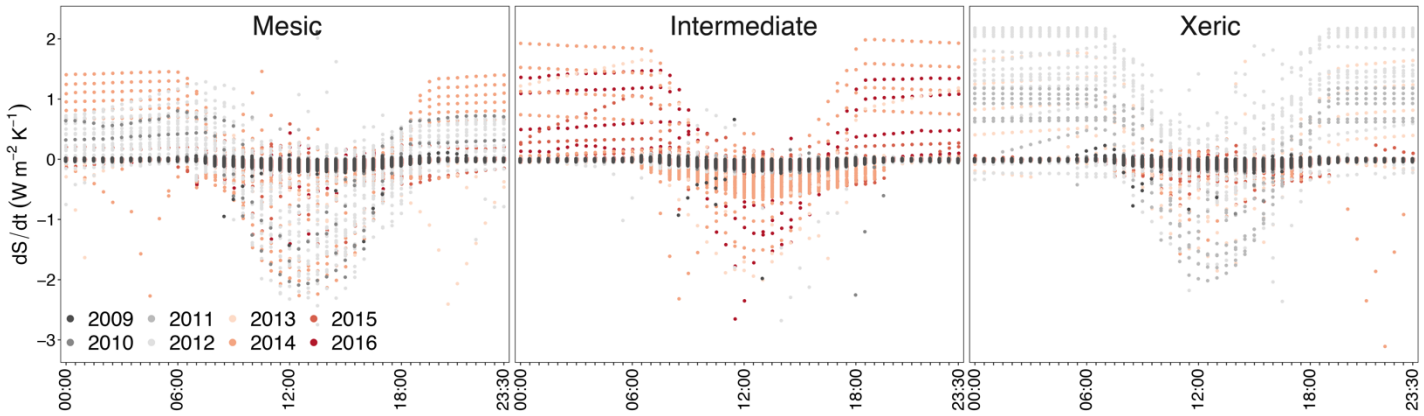

Figure S4: Diurnal changes in entropy (dS/dt) at the mesic, intermediate and xeric sites for the years 2011 through 2016.